Sensitivity of Meteorological variables on Planetary Boundary Layer Parameterization Schemes in the WRF-ARW Model

Anzel de Lange, [*a] Mogesh Naidoo, [b] Rebecca M. Garland, [a,b] Liesl L. Dyson [a]

[a] *Department of Geography, Geoinformatics and Meteorology, University of Pretoria (UP), Hatfield, 0028, South Africa*

[b] *Council for Scientific and Industrial Research (CSIR), Climate and Air Quality Modelling Research Group, Pretoria, 0001, South Africa*

*Corresponding author

E-mail: anzel.delange@up.ac.za

Tel.: +27 82 779 8493

Highlights

- A South African study which investigates the sensitivity of meteorological variables on PBL schemes in the WRF-ARW model.
- There exists variances in meteorological output simulated using difference PBL schemes.
- It is recommended that a local closure PBL scheme be used for the Highveld region during winter.
- During spring, the clearly preferred scheme for the Highveld region is Mellor–Yamada– Janjić (MYJ) PBL scheme.
- Results contribute to the establishment of a preferred PBL scheme for use in South African Highveld region.

Abstract

The accuracy of meteorological fields produced by Numerical Weather Prediction (NWP) models are highly dependent on the physical parameterization schemes used. Any errors in simulations of meteorological fields will be passed on to subsequent processes (i.e. air quality models), and will have an effect on their outputs. Therefore, the realistic simulation of meteorological parameters is of utmost importance. The aim of the present research is to evaluate the performance of Planetary Boundary Layer (PBL) schemes contained in the non-hydrostatic Advanced Research Weather Research and Forecasting (WRF-ARW) model when simulating meteorological variables. Four frequently used PBL schemes were investigated by conducting sensitivity experiments during a month in spring and winter in the South African Highveld

region for 2016. The simulations resulting from the different schemes were compared against one another, and statistically evaluated by making use of observational meteorological data at five sites. From these results, it is recommended that a local scheme be used for the Highveld region during winter. During spring, the clearly preferred scheme for the Highveld is Mellor–Yamada–Janjić (MYJ) scheme. Results from this study contributes to the establishment of a preferred PBL scheme in the WRF-ARW model, for use in South African Highveld region. Future planned research will considered the effect of the above-mentioned PBL schemes in the simulation of air quality over the same region.

Keywords: South Africa, WRF-ARW model, PBL schemes, meteorological simulations, model evaluation

1. Introduction

For decades, meteorological models have been used for the simulation of atmospheric variables (Ritter *et al.,* 2013), and they frequently form part of meteorological research. Numerical Weather Prediction (NWP) models are able to simulate the climate at high resolution, and can be configured with a number of different physics and dynamics options to accommodate different regions and conditions. NWP models are sensitive to many different parameters, and uncertainties in NWP model outputs can be attributed to factors such as the physical parameterizations of atmospheric and surface processes, properties of the domain (size and location), as well as vertical and horizontal resolutions (Crétat *et al.,* 2011; 2012; Crétat and Pohl, 2012). These parameters not only influence resultant meteorological fields, but also have a secondary effect on the outputs from pollution dispersion and air quality models that use these meteorological fields as inputs. Pollution concentration levels fluctuate in response to the changing state of atmospheric stability, associated variations in mixing depth, and the effect of mesoscale and microscale wind systems on the transport and dispersion of air pollution (Tyson and Preston-Whyte, 2000). Therefore, the accurate simulation of meteorological parameters, which are known to have an influence on pollution dispersion and chemistry, is imperative (Gilliam *et al.,* 2006).

Not every parameterization scheme will work well under all circumstances and for all regions, and for this reason it is important for sensitivity experiments to be conducted in order for preferred schemes to be identified. Internationally, a vast amount of research has gone into sensitivity testing of different WRF-ARW model options (such as Planetary Boundary Layer (PBL), radiation, convection, and microphysics schemes, and land-surface models) and their influence on the prediction of meteorological variables (Banks *et al.,*

2016; Borge *et al.,* 2008; Crétat *et al.,* 2012; Giannaros *et al.,* 2019; Hu *et al.,* 2010; Jin *et al.,* 2010; López-Bravo *et al.,* 2018; Ngailo *et al.,* 2018; Politi *et al.,* 2018; Ratna *et al.,* 2014; Zeyaeyan *et al.,* 2017). In South Africa (SA), the simulation of rainfall using the WRF-ARW model with different parameterizations for atmospheric convection has been studied (Crétat *et al.,* 2012; Pohl *et al.,* 2014; Ratna *et al.,* 2014). By testing several physical parameterization schemes, satisfactory configurations of the WRF-ARW model for the regional climate of Southern Africa, particularly with respect to rainfall, was found in Crétat *et al.* (2012). Hahmann *et al.* (2015), when producing the Wind Speed Atlas for SA (WASA), investigated the influence of different physics options on wind speed. Although some research in South Africa has already been conducted with regard to WRF-ARW model parametrization schemes, no comparison of PBL schemes for the Highveld region has been done. In addition, no preferred PBL parameterization scheme for the region has been established.

PBL parameterization schemes are of primary importance when attempting to successfully simulate the boundary layer, and consequently, air pollution concentration levels. These schemes have been used in simulations, compared, and verified against observational data in studies across the world (Banks and Baldasano, 2016; Banks *et al.,* 2016; Boadh *et al.,* 2016; Coniglio *et al.,* 2013; Cuchiara *et al.,* 2014; Gunwani and Mohan, 2017; Hu *et al.,* 2010; Kim *et al.,* 2015; Pérez *et al.,* 2006; Xie *et al.,* 2012). Choice of PBL scheme does not only effect air quality related parameters like mixing height, but also has significant influence on meteorological parameters like temperature, relative humidity, and wind speed and direction. Because different parameterization schemes in models affect the precision of simulated Planetary Boundary Layer Height (PBLH), and other meteorological parameters impacted by PBLH, it is necessary to validate these simulations with measurements (Korhonen *et al.*, 2014).

Deciding which of the PBL schemes to use in an NWP model is not an inconsequential task. Choice of scheme can cause large differences in the simulation of PBLH as found by Banks and Baldasano (2016) over Catalonia, Spain. Not only were there large difference between simulated PBLHs, but different schemes (especially when comparing local and non-local schemes) produced different results for simulated surface meteorological variables as well. These differences in PBLH and meteorological variables between simulations had an influence on the subsequent air quality model outputs. Banks *et al.* (2016) reached similar findings in Athens, Greece, where model simulations produced drastically different results

depending on the PBL scheme used, the meteorological parameter analysed, and the general synoptic conditions. Similarly, in Naigpur, India, the analysis of different meteorological variables show that these are sensitive to the PBL parameterization employed in the NWP model (Boadh *et al.,* 2016).

The main objectives of the presented research is to evaluate the performance of PBL schemes contained in the non-hydrostatic WRF-ARW model (Skamarock *et al.,* 2008). Well-known, frequently used PBL schemes are investigated by conducting various sensitivity experiments during a month in spring (November), and winter (June), in the heavily polluted Highveld region of SA. The simulations resulting from the different schemes are compared with one another, and evaluated by making use of meteorological observations. It is important to accurately simulate meteorological processes, and subsequent pollution events, in regions like the South African Highveld. The significance of this study for the Highveld region is related to the strong relationship between meteorological parameters and air quality. This region is notorious for stable meteorological conditions, which are not conducive to pollution dispersion, especially during winter (Tyson *et al.,* 1988). In terms of air quality, the Highveld region is an air pollution hotspot, where South African National Ambient Air Quality Standards (SA NAAQIS) are regularly exceeded (e.g. Feig *et al.,* 2019; Govender and Sivakumar, 2019; Venter *et al.,* 2012). Thus, a preferred WRF-ARW model setup, and being able to produce accurate NWP model outputs, is of utmost importance for the study region. The results from this study contributes to the establishment of a preferred PBL scheme for use in South African Highveld region.

2. PBL and Surface Layer Scheme (SLS) Options

The WRF-ARW model version 3.8, developed by the National Centre for Atmospheric Research (NCAR), was applied for the meteorological simulations. Version 3.8 of the WRF-ARW model has been extensively used, is stable, and performs well (*i.e.* many of the model bugs have already been eradicated since its release in 2016). In addition, it contains all the schemes and settings required for the presented research.

PBL schemes within the WRF-ARW model parameterize unresolved turbulent vertical fluxes of heat, momentum, and constituents such as moisture within the PBL, and are responsible for turbulent mixing throughout the atmosphere (Hu *et al.,* 2010; Crétat *et al.,* 2012). The PBL, which coincides with the mixing layer, is defined as the lower-tropospheric layer directly adjacent to the surface of the earth. This layer is influenced by the presence of the Earth's surface, and PBL thickness, or height, is dependant thereon (Duda,

2010). PBLH variation has a very strong diurnal pattern. Heights are usually low, and the PBL shallow, during the night when conditions are stable, and can increase to as much as a few kilometres in the noon and afternoon, when solar radiation peaks. These conditions may result in a convective and unstable environment (Liu and Liang, 2010).

In the WRF-ARW model, each PBL scheme is linked to one or more Surface Layer Scheme (SLS). SLS's calculate friction velocities and exchange coefficients (quantitative characteristic of transfer between mediums), which enables the calculation of surface fluxes of momentum, moisture, and heat to the PBL scheme (Banks and Baldasano, 2016; Skamarock *et al.,* 2008).

We expect different results of PBLH and simulated meteorology when using different PBL and SLS parameterization schemes, as each scheme defines and predicts the PBL in a different way. There exist many methods for estimating PBLH. Some schemes use the Bulk Richardson Method, where a critical value (Ri_{cb}) is determined and used to establish the first atmospheric level above the ground, where it (Ri_{cb}) is exceeded by the calculated Richardson number (Ri). This level is then said to separate stable from turbulent atmospheric flow. Another widely used method for defining the top of the PBL is to use turbulent kinetic energy (TKE) or the momentum flux. PBLH is determined at the height at which the value of the relevant variable is lower than a pre-determined critical value (Duda, 2010). Other methods exist, but the two above-mentioned definitions are used in the WRF-ARW model schemes considered here.

Since the performance of PBL schemes when simulating meteorology has not been assessed in the study region, frequently used and well-tested schemes were considered in order to establish a preferred scheme. The Yonsei University Scheme (YSU) (Hong *et al.,* 2006), Mellor–Yamada– Janjić Scheme (MYJ) (Janjić, 1994), Mellor–Yamada Nakanishi Niino Level 2.5 (MYNN) (Nakanishi and Niino, 2006), Asymmetric Convection Model 2 Scheme (ACM) (Pleim, 2007), and their associated SLS's, are investigated in this study (Table 1). These schemes are popular internationally; with the non-local YSU scheme being the most widely used, and the local MYJ scheme following thereafter (Banks *et al.,* 2016). MYNN (local) and ACM (non-local) schemes are also used extensively. The YSU scheme has been used in SA to downscale summer rainfall (Ratna *et al.,* 2014), and summer climate forecasts over Southern Africa (Ratnam et al., 2013), to simulate annual and diurnal cycles of rainfall (Pohl *et al.,* 2014), and when improvements were made to the WRF Seasonal Hindcasts over South Africa (Ratnam *et al.,* 2016). The MYJ scheme was used in a WRF-

Chem modelling study over Southern Africa (Kuik *et al.,* 2015), and when compiling the WASA (Hahmann *et al.*, 2015). Other available schemes were not considered in this study due to their similarity to those mentioned in Table 1. For example, MYNN3 shares characteristics with MYNN, and Quasi-Normal Scale Elimination (QNSE) uses a similar method and threshold to the MYJ scheme (Banks *et al.,* 2016).

These schemes also include local and non-local closure schemes. In a local closure scheme (MYJ and MYNN), a given point is only affected by vertical levels directly adjacent thereto, whereas in a non-local scheme, multiple vertical layers can effect variables at a given point (Cohen *et al.,* 2015). A non-local closure scheme (YSU and ACM) considers several vertical levels when representing the effects of vertical mixing through the PBL.

Table 1. WRF-ARW model PBL schemes, along with their associated SLS's, method of PBLH estimation, and threshold, evaluated in this study. Methods include use of the bulk Richardson number (Ri_b) and turbulent kinetic energy (TKE) (Adapter from Banks *et al.,* 2015).

PBL scheme	Associated SLS	Closure	PBLH method	PBLH threshold
YSU	MM5 similarity	Non-local	Ri_b calculated from surface	0.00 (unstable) and 0.25 (stable)
MYJ	Eta similarity	Local	TKE method and threshold	$0.2\ m^2 s^{-2}$
MYNN	MYNN surface layer	Local	TKE method and threshold	$1.0\ x\ 10^{-6}\ m^2 s^{-2}$
ACM	MM5 similarity	Non-local	Ri_b above neutral buoyancy level	0.25 (unstable and stable)

The TKE (Janjić, 1994; Nakanishi and Niino, 2006), and Ri_b (Hong *et al.,* 2006; Pleim, 2007) methods as used in the PBL schemes in Table 1 are not compatible with observational radiosonde data, and therefore were not be used to estimate the PBLH from observed data. Other methods, described in Section 3.3.2, were considered to derive PBLH from observed radiosonde data.

3. Model description and experimental design

3.1 Study region and case studies

Southern Africa, situated in the subtropics, has a unique air pollution climate. General circulation over this region is dominated by a semi-permanent, subtropical high-pressure cell. Such circulation is associated with divergence and subsidence, resulting in increased stability as well as cloud- and mostly rain-free conditions (Tyson and Preston-Whyte, 2000).

This study focuses specifically on the South African Highveld, which is the portion of the interior plateau of SA, where elevation is above approximately 1500 m above sea level (Fig. 1). The South African Minister of Environmental Affairs has to date declared three pollution priority areas. The Vaal Triangle Airshed Priority

Area (VTAPA) in 2006, and the Highveld Priority Area (HPA) in 2007, were declared as priority areas due to poor air quality caused primarily by industrial emitters, domestic fuel and waste burning, and vehicular sources (DEAT, 2006; 2007). The Waterberg-Bojanala Priority Area was declared in 2012 due to planned development which is expected to adversely impact air quality in the future (DEA, 2012). The HPA and VTAPA are located within the study region. These priority areas experience elevated pollution levels because of many industrial and economic activities concentrated therein, and require specific air quality management action in order to rectify the air quality situation.

According to the Koppen-Geiger climate classification, all sites considered here are classified as temperate. The Highveld region is situated in a summer (December, January, and February) rainfall region, and most precipitation occurs from afternoon thunderstorm during this season. Winters (June, July, and August) in this region are characterised by clear skies, and cold and dry conditions. Conditions for pollutants to disperse are more favourable during spring and summer months (higher mixing heights and unstable atmospheric conditions), while winter conditions tend to inhibit pollution dispersion (lower mixing heights and more stable atmospheric conditions) (De Lange *et al.,* 2019, Tyson and Preston-Whyte, 2000). Due to the contrasting seasonal meteorological conditions in the Highveld region, a winter (June 2016) and a spring (November 2016) case was chosen and used to evaluate the model outputs. As seen in Borge *et al.* (2008), Boadh *et al.,* (2016), Gunwani and Mohan (2017), and Duda (2010), it is common practice to consider different meteorological seasons when evaluating the performance of schemes in the WRF-ARW model.

3.2 Model and Domain

The WRF-ARW model requires two sets of external data to run for a real-data case. Static geographical land-use and surface data from the Moderate Resolution Imaging Spectroradiometer (MODIS) 21 category dataset for the 18km, 6km and 2km domains (Fig. 1), as well as gridded meteorological input data, are used. These are time-varying meteorological fields, and are typically from another regional or global model. We use 6-hourly meteorological input at a 0.2° x 0.2° grid resolution from National Centers for Environmental Prediction (NCEP) Climate Forecast System Version 2 (CFSv2) (Saha *et al.,* 2011). The model run is nudged with NCEP reanalysis data at the outer boundaries on a 6-hourly basis. This process continuously nudges the model towards reality; therefore, day-to-day variations in meteorological conditions are reflected in the simulations (Appendix A).

WRF-ARW model simulations were computed with a month long simulation cycle, excluding a period allotted for model spin-up. Since there is no established definition for the length that a spin-up period should be, a longer (2-week) period was decided on (Jerez *et al.,* 2020). This is to ensure adequate time for the model to stabilize and to counter instability issues within the simulation (Banks and Baldasano, 2016). WRF-ARW model output temporal resolution of 1-h was chosen for purposes of evaluation. Local Time (LT) for the domain is Universal Time Coordinated (UTC) +2.

The WRF-ARW model has multiple physics options, which require a choice of parameterization scheme. All model runs were configured in the same way; therefore, variances in simulated meteorological parameters can be attributed to the chosen PBL and SLS schemes. The simulations in this research were configured as follows: WRF single-moment six-class (WSM6) scheme for microphysics (Hong and Lim, 2006); Kain–Fritsch cumulus parameterization scheme (Kain, 2004); Rapid Radiative Transfer Model scheme for longwave radiation (RRTMG-LW) as well as for shortwave radiation (RRTMG-SW) (Iacono *et al.,* 2008); and the 4-layer NOAH unified land surface model (Tewari *et al.,* 2004). Model simulations are evaluated against observational data, therefore comprehensive schemes for microphysics and radiation were chosen. The remaining model configuration options followed the setup from previous research over Southern Africa (Crétat *et al.,* 2011, 2012; Crétat and Pohl, 2012; Hahmann *et al.,* 2015; Kuik *et al.,* 2015; Pohl *et al.,* 2014; Ratna *et al.,* 2014; Ratnam *et al.*, 2013, 2016).

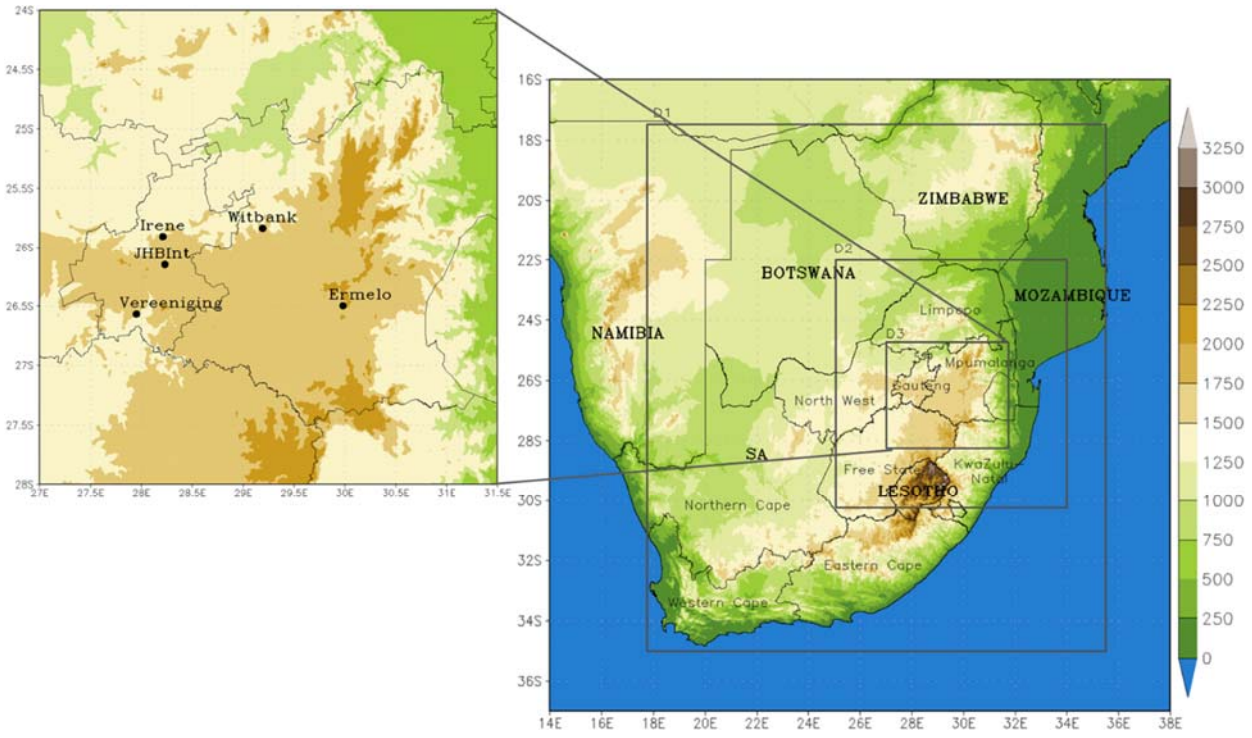

Figure 1. Domains for WRF-ARW model simulations over SA (D1=Domain 1, D2=Domain 2, D3=Domain 3), where the insert shows the five meteorological stations where WRF-ARW model outputs were evaluated. The scale indicates elevation in meters above sea level.

3.3 Data for model evaluation

Meteorological variables, which greatly affect the dispersion and diffusion of pollutants in the atmosphere (Brunner *et al.,* 2015), are evaluated. These are temperature; relative humidity (RH); wind speed and direction; and PBLHs.

3.3.1 Meteorological data

Meteorological measurements were obtained from the South African Weather Service (SAWS). SAWS has a countrywide observational network of weather stations with hourly data for, amongst others, temperature, RH, wind speed and wind direction. These data were used to verify interpolated outputs from the WRF-ARW model at five stations located in Domain 3 (Fig. 1). These five meteorological stations were chosen based on their location in the Highveld region, and data availability. The locations of the five stations, which includes three weather offices (Irene, Ermelo, Johannesburg International Airport), and two automated weather stations (Vereeniging and Witbank), are indicated in Figure 1. Data availability for the period is more than 95% for all variables at all stations, except wind speed and direction for June and

November 2016, and RH for November 2016 at Vereeniging, where no data were available. These variables at Vereeniging were therefore not considered in the results.

3.3.2 Radiosonde

PBLH is a meteorological parameter that is not directly measured, but estimated or derived using meteorological observations at different vertical levels. The accurate representation of PBLH in the WRF-ARW model is essential, not only for the simulation of meteorological conditions within the boundary layer, but also for simulating air quality. The overestimation of the PBLH might lead to the underestimation of air pollutant concentrations modelled with the air quality models, whereas an under-estimation may have the opposite effect (Kryza *et al.,* 2015).

In this study, PBLH is estimated from available observed sounding data in order to compare to the four PBLH simulations (Table 1). Data are available at several levels from the radiosonde launches performed at SAWS weather station at Irene (Fig. 1). This is the only operational upper air station in the domain, and may be considered a proximity sounding, and representative of atmospheric conditions in the Highveld region (Dyson *et al.,* 2015). The radiosonde records barometric pressure, temperature, RH, wind speed and direction. Potential temperature was calculated from these variables.

Soundings are done twice a day, at midnight (00 UTC/ 02 Local Time (LT)) and midday (12 UTC/ 14 LT). SAWS supplied 82 soundings for June and November 2016. Eight soundings in total were removed from the data set. Three of these did not pass the quality control procedures and were removed because of failing the fundamental sanity check as described by Dyson *et al.* (2015). There were only two mid-day soundings in June 2016, which were not considered as they are not representative of the entire period. In three of the soundings, there was no PBL that met the requirements for either the Holzwoth method nor SBI method as explained in Figure 2. While the lack of useable midday soundings during the June 2016 period is not ideal, it has only a minor influence on the verification statistics presented, and not on the model results. In addition, PBL heights during winter in the study region do not vary much from day-to-day because of prevailing meteorological conditions.

Table 2 indicates the number of usable soundings after quality control, and where either a Stable Boundary Layer (SBL) (00 UTC/ 02 LT) or a Convective Boundary Layer (CBL) (12 UTC/ 14 LT) height could be

identified. There were no usable soundings available at midday during June 2016, but good availability of soundings for the spring case for both times.

Table 2. Useable radiosonde data for the period June 2016 and November 2016. Numbers in brackets indicate the original number of soundings received from SAWS for every case.

	12UTC sounding	00UTC sounding	Total
June 2016	0 (2)	20 (23)	20 (25)
November 2016	28 (28)	26 (29)	54 (57)

Observed planetary boundary layer height (OPBLH) is defined in this study as in Hu *et al.* (2010), who stated that "PBLH is the height of the top of the layer within which vigorous vertical mixing is taking place, otherwise known as the mixing height." Since the mixing layer corresponds to the PBL (Seibert *et al.,* 2000), OPBLHs can be derived from the radiosound data using the simple parcel method (Fig. 2; left). This method, also sometimes referred to as the "Holzworth method", was developed in 1964 when Holzworth conducted a study estimating maximum mixing depths for radiosonde stations across the United States (Holzworth, 1964). This approach requires vertical profiles of potential temperature, as well as accurate surface temperatures. The height of the mixing layer is defined as the height where potential temperature is equal to the potential temperature at the surface (Collaud Coen *et al.,* 2014). This method is only applied when CBL is present, it is not used at night when the nocturnal SBL prevails (Seibert *et al.,* 2000).

A second method was used to calculate the height of the SBL, which prevails from sunset to sunrise. According to Collaud Coen *et al.* (2014), the SBL is characterized by the surface-based temperature inversion. The top of this inversion can be estimated by at the height where potential temperature change has a gradient equal to zero. In this article, the first level above the ground where potential temperature gradient was less than 0.5 and a temperature inversion (or isothermal layer) was present, was considered to be the top of the SBL. This method is hereafter referred to as the surface-based temperature inversion (SBI) method (Fig. 2; right).

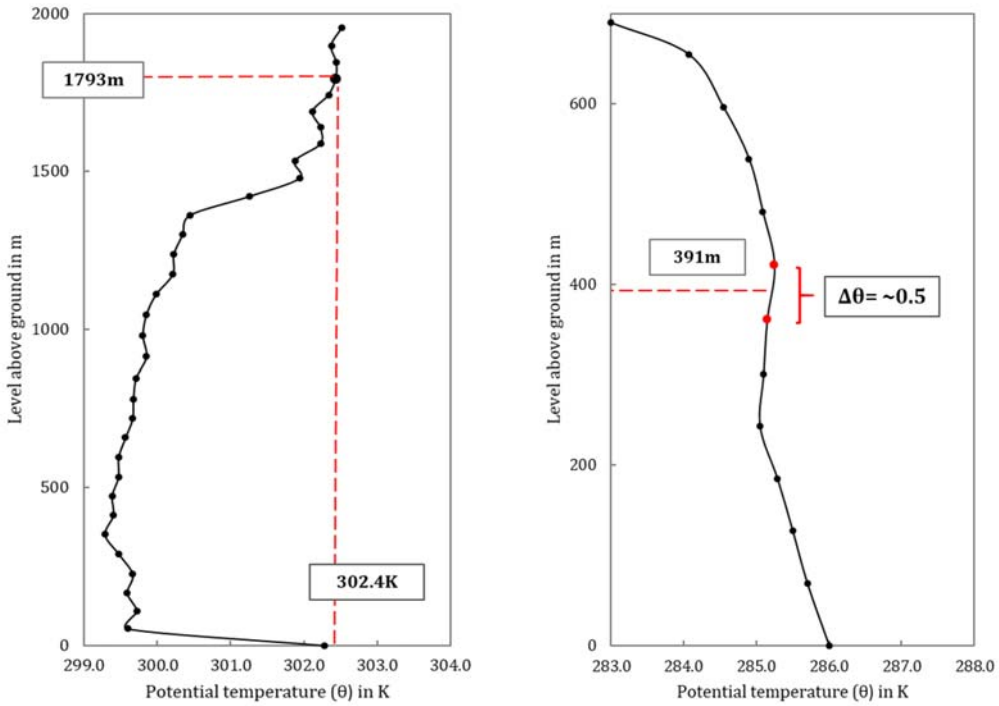

Figure 2. Examples of calculation of the OPBLH, based on the parcel method for CBL (left), and the SBI method for SBL (right), conditions. The x-axis shows potential temperatures (θ) and the y-axis, height (in m) above ground level. The height of the OPBLH is indicated by a red line on the y-axis. On the left graph the surface potential temperature (302.4K) is depicted by the red line. The surface potential temperature is only reached again at 1793 m above the ground, which is the OPBLH (Holzwoth method). In the graph on the right, the red lines indicates the midpoint between two levels, where potential temperature gradient is less than 0.5 K. The OPBLH in this example is 391 m above ground level (SBI method).

Seibert *et al.* (2000) noted that "Reliable mixing height determination under all conditions is therefore still an unsolved problem." It is important to bear in mind that although radiosonde data are considered adequate to estimate the SBL/CBL (100-500m) and CBL (500-3000m) heights, it struggles to estimate low SBL (10-100m) heights (Seibert *et al.,* 2000). While we present methods where CBL as well as SBL heights are estimated, these heights are considered approximations only, especially during periods when low SBLs occur (i.e. winter period at 00 UTC).

3.4 Model evaluation

Model evaluation is performed for WRF-ARW model simulated surface temperature, RH, wind speed, wind direction and PBLH. These variables were compared with observed surface values and sounding-derived PBLHs (Fig. 2). The simulated PBLHs are compared with OPBLH at 02 and 14 LT only. Visual and statistical evaluations are performed for the four different PBL schemes in WRF-ARW model. Statistics used in the

verification of the simulation results include Pearson product-moment correlation coefficient (R), Bias, Index of Agreement (IOA), and Mean Absolute Percentage Error (MAPE).

4. Meteorological simulations and verification

We present the results for the verification of the surface variables for June and November 2016 in Section 4.1 to 4.3. In Section 4.4, PBLHs from the different PBL schemes in the WRF-ARW model are compared with one another, and the OPBLHs derived from the sounding data at Irene. Section 4.5 presents a summary of the results found.

4.1 Temperature

The MYNN PBL scheme performs well with respect to average temperature simulation (not shown). In almost 50% of cases, this scheme simulated average temperatures to be the most similar to the observed. This scheme was especially accurate at Ermelo, Vereeniging, and Witbank. MYNN is outperformed at the two remaining sites, Irene and JHB Int., where ACM and MYJ also performed relatively well. Average daytime (06 to 17 LT) and night-time (18 to 05 LT) temperatures are a good indication of the periods when specific model setups work well. For the purposes of this study, an absolute temperature bias of less than 2 °C is considered a "good forecast" (Colman, n.d.). Most schemes over-estimated temperatures during day and night-time, as well as average daily maximum temperatures, with the exceptions at Irene. Minimum temperatures are fairly well simulated at all sites except at Vereeniging, where they are over-estimated by more than 2°C.

The relationships between observed and simulated temperatures in June are strong with R-values >0.88 for all schemes at all sites (Table 3). The best performing scheme in terms of average biases is MYNN, with MYJ and ACM also performing well at certain sites. The site where simulated temperatures performed best overall is JHB Int. Here, average biases are all less than 0.65°C, and there is very high agreement between observed and simulated temperature (IOA>0.95). From the statistics presented, it is evident that accuracy when simulating temperatures is fairly site-specific in terms of the PBL schemes. For instance, MYNN is the best performing scheme (averages, bias, R, IOA and MAPE) at three of the sites, but at Irene and JHB Int. MYNN is often one of the worst-performers. While this is true, the scheme still performs well at these sites with relatively low biases and high scores for R, IOA and MAPE.

For November (not shown), the scheme with the most accurate average temperatures (period, daytime and night-time) is MYJ. This scheme is the best performer at all sites, except at Irene, where ACM is. Average daily maximum temperatures were over-estimated by all model setups at all sites by 2°C on average. Average minimum temperatures were also over-estimated in most cases, but to a lesser extent. The standout PBL scheme with respect to average temperature is MYJ. In more than 75% of cases, this scheme simulated average temperatures to be the most similar to the observed. ACM does perform particularly well at Irene, especially in terms of night-time and daytime averages. MYNN, which was the best performing scheme in terms of averages for June, only outperforms the MYJ scheme on occasion. In terms of the performance indicators (not shown), relationships between observed and simulated temperatures in November are strong ($R>0.79$) for all schemes at all sites. In June, the weakest correlations are found at Vereeniging. Vereeniging also produced the weakest correlations, largest biases, lowest IOA scores, largest MAPE for the period.

The average hourly temperature biases for one of the best performing sites, Ermelo (where average absolute bias in June was $<2°C$), are plotted in Figure 3 (top). Temperature biases are similar in magnitude at all sites (not shown) with the exception of Vereeniging, where hourly temperature biases were high (with hourly values of close to 10°C in some cases). Considering all the sites, temperature biases show no clear diurnal pattern during June, and the over-prediction and under-prediction of hourly temperatures happen at different times of the day at each site. It is interesting to note at Ermelo that MYNN under-predicts temperature for a few hours in the early morning, while all other schemes over-predict temperatures throughout the day. The only site where temperatures are over-predicted by all schemes for the entire day was at Vereeniging, where average hourly temperature bias ranges from approximately 1°C during midday (10 to 17 LT) to 4°C during the rest of the day. There is no single best performing PBL scheme in terms of hourly temperature biases for all sites during June. MYNN performs best at Ermelo, Vereeniging and Witbank, MYJ at Irene, and YSU and ACM at JHB Int. and Witbank.

During November, most schemes tended to under-predict temperature during the night and up to noon (approximately 12 LT), and over-predicted temperatures when temperatures typically cool down in the afternoon. In November, at Ermelo (Fig. 3; bottom), the MYJ scheme produced the smallest average hourly biases, and reached a maximum ($+2.4°C$) at 13 LT. MYNN and ACM have largest average biases at this site,

and are outperformed by YSU, especially in the evening (17 to 21 LT). During November, the MYJ scheme produced the lowest hourly biases, and therefore the most accurate hourly temperature simulations, at all sites except Irene, where ACM was the most accurate

Table 3. Performance indicator results for hourly temperature simulated with the WRF-ARW model using different PBL schemes (YSU, MYJ, MYNN and ACM) for June. Underlined values indicate best score for each indicator.

Station	Performance indicator	YSU	MYJ	MYNN	ACM
Ermelo	R	0.95	0.95	0.93	0.95
	Bias	1.01	1.22	0.44	1.05
	IOA	0.96	0.96	0.96	0.96
	MAPE (%)	18.69	21.23	18.53	18.99
Irene	R	0.96	0.95	0.94	0.96
	Bias	-1.03	-0.15	-1.79	-1.05
	IOA	0.97	0.97	0.93	0.97
	MAPE (%)	12.11	9.42	16.26	12.12
JHB Int.	R	0.92	0.93	0.91	0.92
	Bias	-0.12	0.64	-0.56	-0.06
	IOA	0.96	0.96	0.95	0.96
	MAPE (%)	13.04	13.42	14.88	13.33
Vereeniging	R	0.93	0.88	0.92	0.93
	Bias	2.47	3.38	1.74	2.50
	IOA	0.91	0.85	0.93	0.91
	MAPE (%)	129.32	185.79	103.72	129.03
Witbank	R	0.94	0.92	0.91	0.94
	Bias	0.95	1.58	0.26	0.98
	IOA	0.96	0.93	0.95	0.96
	MAPE (%)	15.58	21.47	17.00	15.89

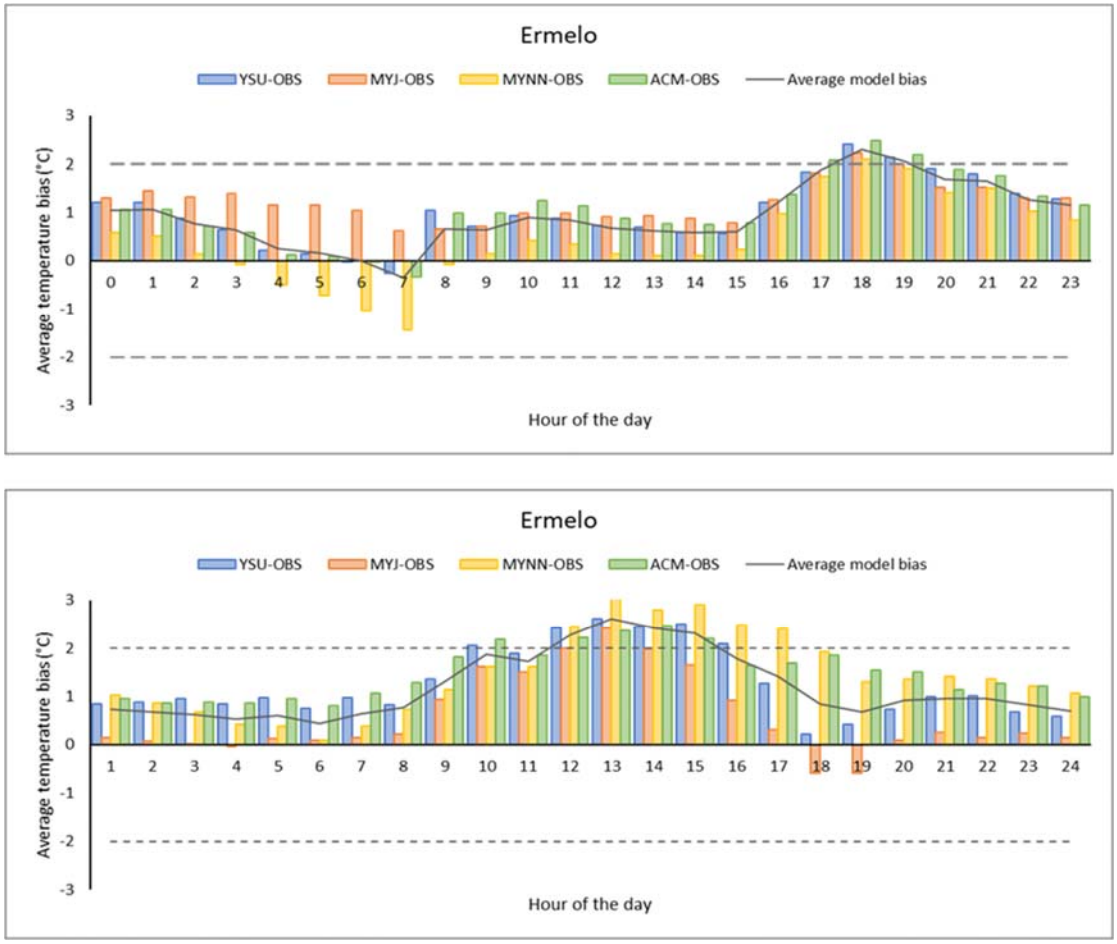

Figure 3. Average temperature bias (Modelled – Observed temperature) calculated for each hour and experimental setup at Ermelo during June (top) and November (bottom). Average bias of + and - 2 °C is indicated (----).

4.2 Relative Humidity

At all the sites in November the RH peaks in the early morning (between 04 and 06 LT) and drops to a minimum (~50% on average) from approximately 14 to 15 LT (Fig. 4). Although RH is visibly under-estimated from late-morning to the afternoon, the diurnal pattern of RH is simulated relatively well in all model setups (Fig. 4). YSU, MYNN, and ACM, which has the largest temperature biases in the late afternoon at Ermelo (Fig. 3; bottom), under-predicts RH values the most (Fig. 4; top left). MYJ has the lowest temperature biases in the late afternoon and evening on Fig. 3 (bottom) and also has the lowest biases in RH during this period (Fig 4; top left), even showing an over-estimation of RH at night. The relationship between temperature and RH is inversely proportional (Wallace and Hobbs, 2006). This relationship is shown in the results of Figure 3 and 4.

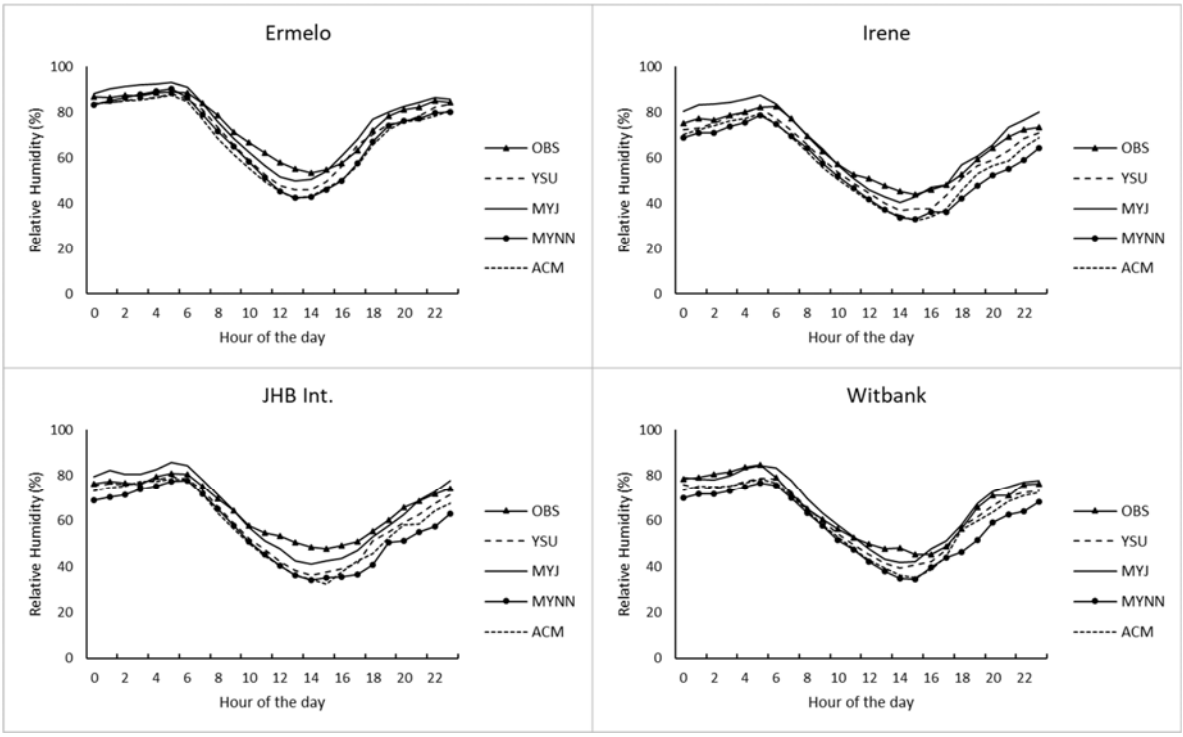

Figure 4. Average hourly RH (%) at each site for November.

June observations (not shown) indicate peak RH values at approximately 07 LT at all sites and a low (~30% on average) between 14 and 16 LT. The simulated RH values reproduced the June diurnal RH pattern well, although RH is under-estimated most of the time (as it is in November). At Vereeniging, Irene and Witbank, RH is under-estimated in the late afternoon and evening in all the simulations.

Correlations for November are relatively low (Table 4), ranging from 0.67 (Witbank; MYNN), to as high as 0.79 (Ermelo; MYJ and MYNN). Schemes that stand out as best performing for November are MYJ, with YSU second, while MYNN and ACM are clearly the worst-performers. Biases are mostly negative, meaning that RH is on average under-estimated. IOA is relatively high, with a scores of more than 0.79 for all cases. June correlations (not shown) are all high ($R>0.79$), indicating strong agreement between modelled and observed RH at the considered sites. High correlations were expected because of the strong diurnal pattern associated with RH. Biases are mostly negative, with the largest average biases at Vereeniging. Performance indicator results reveal YSU as the best performer when RH is simulated for June. Bias is the only test where YSU is outperformed by other PBL schemes. MAPE ranges from 16.90% (Ermelo; YSU) to as high as 22.82% (Vereeniging; MYNN).

In the diurnal, average hourly RH is under-estimated by all PBL schemes during certain periods of the day at most of the sites (Irene, JHB Int., Vereeniging, and Witbank), during June. Considering that RH is a function of temperature, these under-predictions of RH frequently coincide with over-predictions of temperature. A similar under-estimation of RH is also seen during November (Fig. 4). Here, on average, lower RH was commonly simulated in the noon and afternoon, and at JHB Int., into the evening. These under-estimations of RH also often coincide with hours where temperature biases were positive.

Table 4. Performance indicator results for RH simulated with the WRF-ARW model using different PBL schemes (YSU, MYJ, MYNN and ACM) November. Underlined values indicate best score for each indicator.

Station	Performance indicator	YSU	MYJ	MYNN	ACM
Ermelo	R	0.78	0.79	0.79	0.78
	Bias	-4.24	0.52	-5.50	-6.86
	IOA	0.86	0.89	0.86	0.84
	MAPE	16.08	13.28	16.40	17.75
Irene	R	0.78	0.74	0.74	0.76
	Bias	-4.05	1.83	-8.40	-7.16
	IOA	0.87	0.86	0.82	0.84
	MAPE	19.45	19.56	21.78	21.32
JHB Int.	R	0.77	0.70	0.73	0.74
	Bias	-5.24	-0.45	-9.29	-7.25
	IOA	0.86	0.84	0.81	0.83
	MAPE	20.35	19.92	22.50	22.81
Witbank	R	0.68	0.73	0.67	0.70
	Bias	-3.39	0.53	-7.80	-5.09
	IOA	0.82	0.85	0.79	0.82
	MAPE	18.77	17.07	20.70	19.76

4.3 Wind speed and direction

During June, strong relationships between observed and simulated wind speeds ($R>0.66$) were present for all schemes at all sites (Table 5). Biases for all simulations at all sites are on average less than $\sim 1 ms^{-1}$. In terms of all performance indicator results, MYNN performs well at Ermelo, whereas MYJ produces some good results for the remaining sites. Overall, performance between schemes were very similar when considering only performance indicator results.

November relationships between observed and simulated wind speeds (not shown) are not as strong as during June, with correlations ranging from as low as 0.33 (Witbank) to 0.44 (Irene). Biases for all simulations at all sites are on average larger than ~ 1 ms^{-1}, with the largest average bias for a model setup being 2.36 ms^{-1} (Witbank with YSU scheme). When considering all performance indicator results, the scheme that produced the most accurate wind speeds across all sites was MYJ, although ACM did outperform MYJ in terms of bias and MAPE at Irene.

Average wind speed frequency of occurrence for Ermelo is plotted in Figure 5. The wind speed distribution is well simulated by all setups during June. At Ermelo in June (Fig. 5; top), wind speed class 4 to 5 ms^{-1} is over-estimated, while the most frequent occurring classes (2 to 4 ms^{-1}) are simulated well by all schemes. When considering all June results, MYJ is the scheme that produced the most accurate wind speeds at most of the sites except Ermelo, where ACM performed best on average. During November, at Ermelo (Fig. 5; bottom) the frequently occurring wind classes of 4 to 7 ms^{-1} winds are over-estimated by all but one scheme.

The hourly average wind speed biases for all schemes for June at Ermelo (Fig. 6; top) is mostly negative, indicating that the observed winds are stronger than the simulated winds. However, the absolute bias values are generally all less than 1 ms^{-1}. Average June wind speed bias at Ermelo is only -0.44 ms^{-1} (Table 5). These low bias values are present at all the stations, but no clear diurnal patterns are present. In November, all schemes overestimate the wind strength at Ermelo, with the largest biases at night by YSU, MYJ, and MYNN (Fig. 6; bottom). The average bias at Ermelo in November is 1.6 ms^{-1}. Mostly positive biases are present at all sites in November.

Table 5. Performance indicator results for wind speed simulated with the WRF-ARW model using different PBL schemes (YSU, MYJ, MYNN and ACM) June. Underlined values indicate best score for each indicator.

Station	Performance indicator	YSU	MYJ	MYNN	ACM
Ermelo	R	0.72	0.73	<u>0.75</u>	0.72
	Bias	-0.32	-0.62	-0.52	<u>-0.28</u>
	IOA	<u>0.84</u>	0.82	<u>0.84</u>	<u>0.84</u>
	MAPE (%)	29.70	29.64	<u>27.92</u>	29.49
Irene	R	<u>0.72</u>	0.71	0.68	0.69
	Bias	-0.33	<u>0.15</u>	-0.36	-0.21
	IOA	0.82	<u>0.83</u>	0.80	0.81
	MAPE (%)	40.10	<u>36.64</u>	40.35	41.47
JHB Int.	R	<u>0.67</u>	<u>0.67</u>	0.66	0.65
	Bias	-0.23	-0.45	-0.30	<u>-0.20</u>
	IOA	<u>0.81</u>	0.78	0.79	0.80
	MAPE (%)	34.22	<u>32.46</u>	35.16	35.32
Witbank	R	0.73	0.73	<u>0.74</u>	<u>0.74</u>
	Bias	0.38	<u>0.21</u>	0.40	0.33
	IOA	0.84	<u>0.85</u>	<u>0.85</u>	0.84
	MAPE (%)	42.13	<u>35.41</u>	38.83	40.25

Average wind direction frequency of occurrence for Ermelo is plotted in Figure 7. All the schemes performed very well in simulating wind direction at Ermelo in June (Fig. 7; top). The only exceptions are the 270° to 315°direction, where all the schemes have higher frequencies than observed and the 315° to 360° direction, where all the schemes have a lower frequency. In the case of November (Fig. 7; bottom),

the observed dominant wind direction is in the Northerly quadrant (45° to 315°), which is somewhat over-estimated by most model setups. Nevertheless, the overall pattern of wind direction occurrence is reproduced well at this site. MYJ again stands out as the scheme that most frequently simulated wind directions in their observed classes.

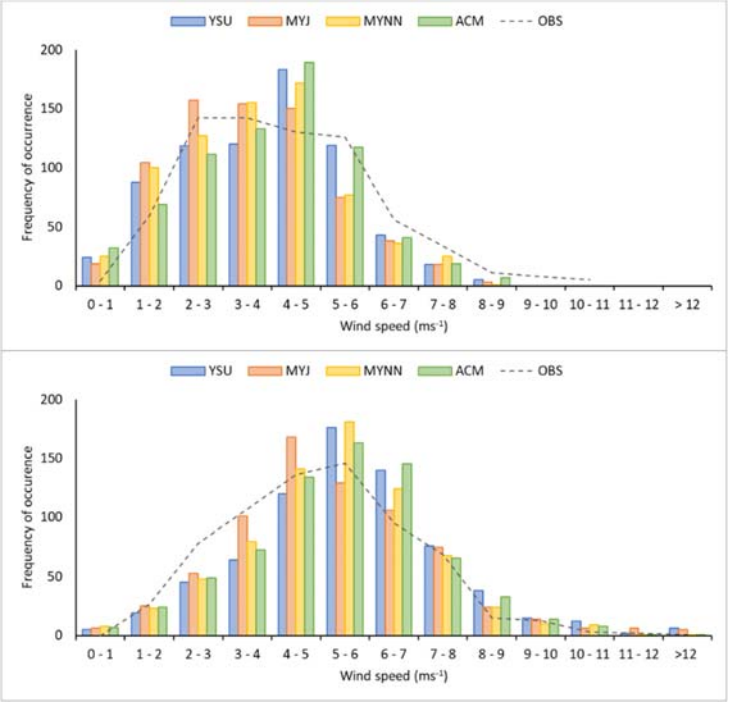

Figure 5. Frequency of occurrence of wind speed for June (top) and November (bottom) in specified classes at Ermelo.

Considering all the schemes, the wind speed distribution are not as well simulated as wind direction, and the most frequent wind speed class are only reproduced by the simulations on occasion. The MYJ scheme was generally the most successful in correctly simulating hourly wind direction classes during June for all sites. The schemes with the most hours simulated in the correct classes during November is MYJ at Ermelo, JHB Int., and Witbank, while MYNN performed well at Irene (not shown).

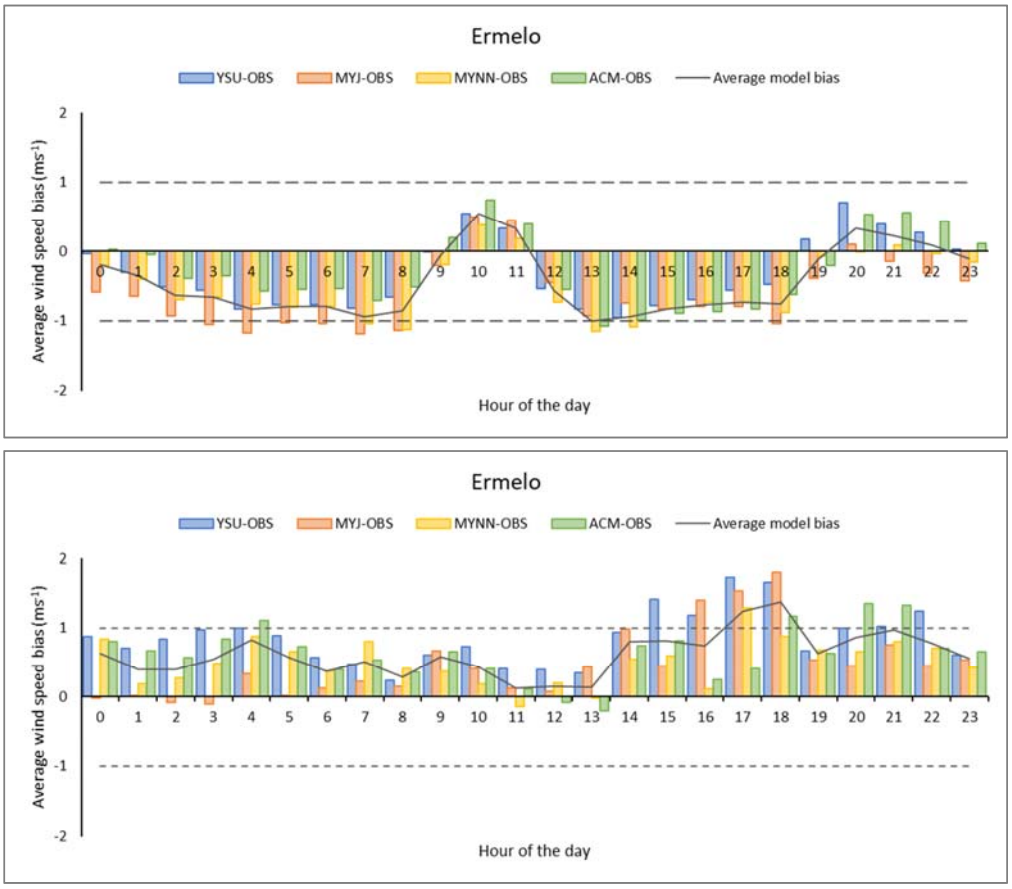

Figure 6. Average wind speed bias (Modelled – Observed temperature) calculated for each hour and experimental setup at Ermelo, during June (top) and November (bottom). Average bias of + and - 1 m.s^{-1} is indicated (----).

4.4 Planetary Boundary Layer Height

Radiosonde data was available at only one of the five sites, therefore PBLHs are only compared at Irene, and only at 00 UTC and 12 UTC (when soundings are performed). Following the discussion in section 3.2.2, the OBLH was calculated from potential temperatures by using the two named methods. A direct comparison between OPBLH and the PBLHs simulated by the four schemes is therefore not possible. Nevertheless, for June at 02 LT (Fig. 8; top), the simulated SBL heights is slightly lower than the OPBLH. On average, there is less than a 50m difference between the OPBLH and the PBLHs modelled by the two best performing schemes (MYJ and MYNN).

In November (Fig. 8; bottom) the simulated PLBH are higher than the OPBLH at both 02 LT and 14 LT. The largest differences occur in the CBL at 14 LT. On average, the ACM scheme produces the OPBLH closest to the derived for the midnight sounding with only a 63m over-estimation. During the day, when all schemes over-estimated the 14 LT OPBLH, YSU was the best performing, over-estimating the PBLH by less than 300m.

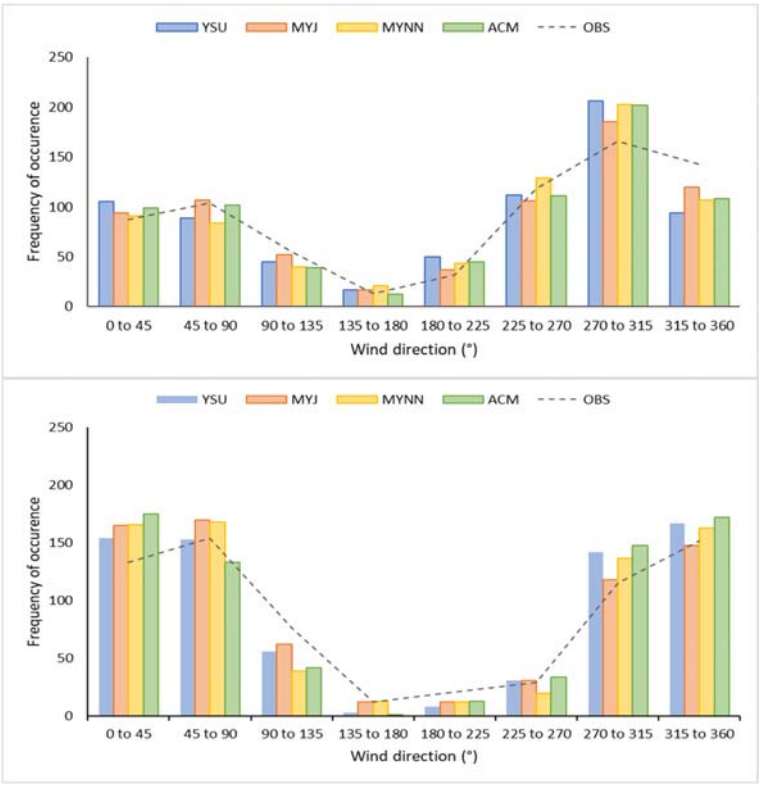

Figure 7. Frequency of occurrence of wind directions for June (top) and November (bottom) in specified classes at Ermelo.

November PBLHs at the different sites varied on average from lows of between 150m and 600m, to highs of between 1700m and 2300m (Fig. 8 and 9). PBLH minimums are mostly reached in the early morning hours (between 06 and 08 LT), but minimum heights are predicted to occur in the late evening (from 18 and 20 LT), by MYJ at Irene, JHB Int., and Vereeniging. Maximum PBLHs during November were simulated to occur between 13 LT and 15 LT; this is when solar radiation peaks, and vertical mixing are at their most vigorous. On average, MYJ produces the highest PBLH for November across all sites, and YSU the lowest. Although the MYNN scheme does not show the highest peak values in the diurnal cycle, it simulates the break-up of the CBL at a slower rate than the other schemes, and therefore, on average has the highest PBLHs.

June simulated PBLHs varied from lows between 50m and 300m, to highs of between 1300m and 1900m (not shown). Average maximum June PBLHs are simulated to occur between 14 LT and 17 LT. On average, MYNN produces the highest PBLH for June period across all sites.

PBLH simulated by the WRF-ARW model are at a minimum throughout the night (>500m during winter, ~500m during spring), increases from 08 LT, and reaches a peak during the afternoon. This pattern is fairly

similar for all schemes, except MYNN during June. PBLH simulated by MYNN tend to peak later and drop to the nightly minimum more gradually than the other sites, on average. Generally, ACM predicts the maximum PBLH the latest in the afternoon, but with a sharp decrease in values after the peak. MYJ simulates its maximum PBLH earlier in the day, with a more gradual decrease in heights in the afternoon and evening. There is good parity between PBLHs simulations during the day between YSU and MYNN. Even though the minimum values of PBLHs are simulated at different heights, they all show an increase in height after 08 LT, the decrease in heights after the maximum values are more uncertain.

Important to note is that PBLH is a function of temperature, the frequent over-estimation of temperature during June and November (section 4.1) is likely to cause some over-estimation of PBLHs. On average, the local PBL schemes, MYJ and MYNN produce the highest PBL for November and June, respectively. The two local schemes (MYNN and MYJ) use the TKE method for the calculation of PBLH, while the two non-local schemes (YSU and ACM), and use the Bulk Richardson method.

This section provides a general idea of the performance of the WRF-ARW model when simulating PBLHs. The observational data used for verification lacked temporal resolution, and therefore no conclusion regarding the best performing scheme in terms of simulating PBLH can be made at this stage. Worth mentioning is that the two local schemes (MYJ and MYNN) produced PBLHs closer to the derived PBLH during June, and the two non-local schemes (YSU and ACM) during November.

While a radiosonde records many variables (barometric pressure, temperature, RH, wind speed and direction), vertical profiles of potential temperature were considered for further analysis (Appendix B) as potential temperature profiles were used in the derivation of PBLHs. In terms of June soundings (02 LT), potential temperature profiles simulated by the different schemes are very similar, and at times near identical, throughout the atmosphere from 850 to 700 hectopascal (hPa). On average, potential temperature is under-estimated, and average biases are very small, less than 0.2 Kelvin (K) for all schemes (Fig. B.1). Overall, the observed potential temperature profile is reproduced very well by all schemes during June (02 LT), except for a surface inversion at approximately 830hPa, which is not reproduced in the simulation.

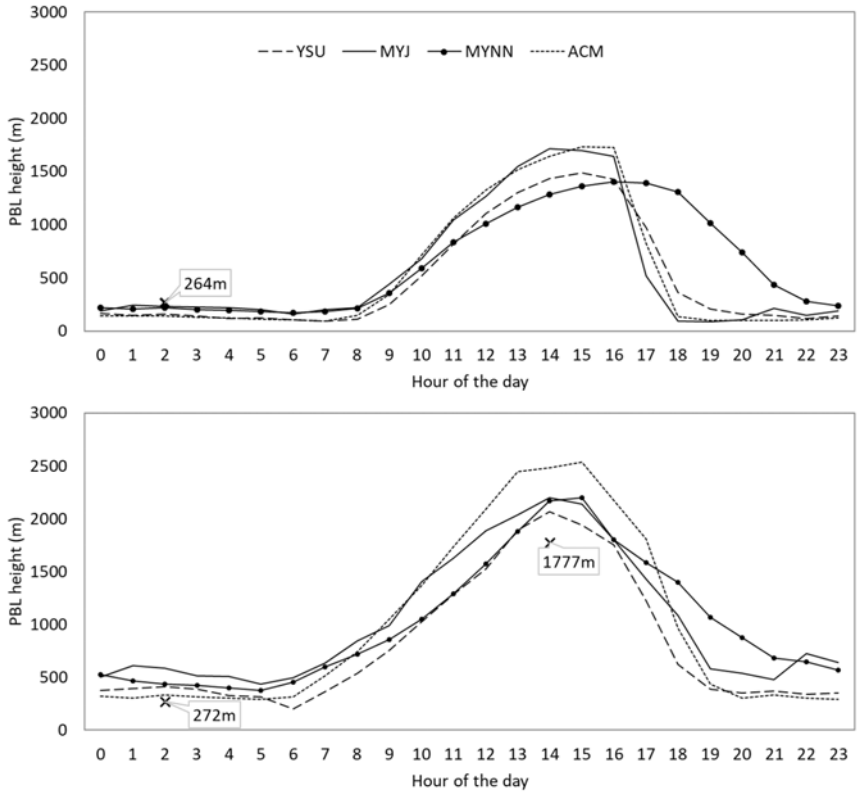

Figure 8. Average hourly PBLH simulated by each model setup at Irene during June (top) and November (bottom). OPBLH derived from sounding data is indicated (X) at 02 and 14 LT when available.

During November (02 LT) the observed potential temperature pattern is reproduced well, but on average, under-estimated (Fig. B.2). As with the June (02 LT) case, average biases are small, less than 0.7 K, with the largest biases being present in the upper-atmosphere (750hPa and higher; not shown). Variation between simulated potential temperature profiles for the November at 14 LT are larger than those during November at 02 LT. These variations in potential temperature profiles are caused by frequent over-estimation of surface temperature at the time of the sounding. In terms of November 14 LT soundings (Fig. B.3), potential temperature is primarily over-estimated in the lower layers, with biases becoming smaller in the upper atmosphere (not shown). The over-estimation of potential temperatures in the lower levels, as well as the fluctuating pattern of the observed potential temperature profiles, led to considerably different PBLHs being simulated, and derived, in Figure 8 (bottom). As the schemes performed relatively similar, no one scheme stands out as the best performing across all cases when reproducing vertical potential temperature profiles.

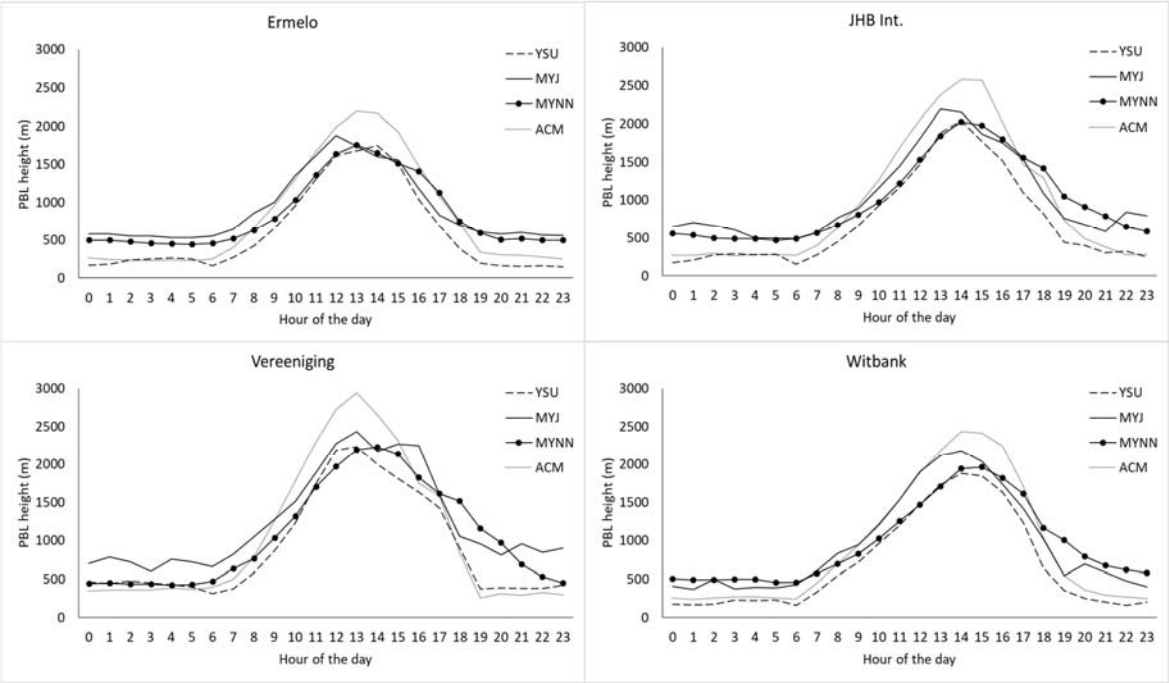

Figure 9. Average hourly PBLH simulated by each model setup at Ermelo, JHB Int., Vereeniging, and Witbank during November.

4.5 Summary

Relationships between simulated and observed temperatures for June were strong, with correlations ranging between R=0.88 to R=0.96, while November correlations ranged between R=0.79 to R=0.87. Average temperature biases for June were less than roughly 2°C for all sites except Vereeniging, where biases were large. In terms of PBL schemes, MYNN performed well at Ermelo, Vereeniging and Witbank, while MYJ produced the most accurate temperature simulations at Irene, and ACM at JHB Int. The standout PBL scheme with respect to average temperature simulation, during November was MYJ. MYJ also produced the most accurate hourly temperature simulations for most sites during this period.

In terms of RH, June correlations in are all high (R>0.79), indicating strong agreement between modelled and observed RH at the considered sites. Performance indicator results for this period reveal YSU as the best performer. During November, RH is under-estimated from late-morning to the afternoon in most cases. Temperatures being mostly over-estimated constitutes one of the factors contributing to this under-estimation of RH. Schemes that stand out as best performing during November are MYJ, with YSU second, while MYNN and ACM are very clearly the worst performers.

Hourly biases for wind speed were on average less than 1 ms^{-1}, and performance indicator results were very similar between different model setups. MYJ is considered one of the best performing PBL schemes in accurately simulating the occurrence of different wind speed and direction classes. November simulations of wind speeds were the worst performing of the meteorological variables. Correlations were low (ranging from 0.33 to 0.44), and biases for all simulations at all sites were on average larger than ~1 ms^{-1}. When considering all performance indicator results, the scheme that produced the most accurate wind speeds across all sites was MYJ for November. Overall, the WRF-ARW model, with all tested configurations, tended to reproduce all surface variables more accurately during the winter period than during the spring.

Expected diurnal variation of PBLHs was reproduced well by the schemes in the WRF-ARW model. In terms of PBLH, the local schemes (MYJ and MYNN) on average produced the highest PBL for November and June. MYJ and MYNN simulated PBLHs closer to the average derived PBLH at Irene during June, while YSU and ACM schemes performed best during the November.

5. Discussion

Results from this study indicate that the accurate simulation of meteorology with different PBL schemes is not only site-specific, but also variable-specific. For instance, while a local scheme like MYJ/MYNN is recommended in the Highveld region during June, the non-local YSU scheme outperformed the local schemes in simulating RH during this period. Therefore, as advised by Gunwani and Mohan (2017), it is suggested that the scheme used in a study ought to be based on the meteorological parameter to be studied, as well as the climatic zone under consideration.

While an overall suggestion for types of schemes to use during winter and spring in the Highveld region can be made, no single best performing option across sites and seasons was identified. This conclusion is common when considering WRF-ARW model verification studies. For instance, Gunwani and Mohan (2017), examined five PBL schemes to find no clearly best performing option for the different climatic zones of India. In an article by Cuchiara *et al.* (2014), simulated vertical profiles for some meteorological variables were compared to measurements collected in Texas during summer 2006; again, the overall results did not indicate any preferred PBL scheme. In a 2010 article written by Hu *et al.,* three PBL schemes were evaluated over south-central United States, where it was found that simulations with the YSU and ACM schemes give much less bias than with the MYJ scheme. In the 2016 study by Boadh *et al.,* the authors

concluded that out of the five PBL schemes (three local and two non-local) considered, the non-local PBL scheme YSU, followed by local scheme MYNN, may be able to capture the characteristic variations of surface meteorological variables and the thermodynamic structure of the atmosphere over Nagpur, India. Banks *et al.* (2016) considered eight different PBL schemes and tested those using daily simulations on a 1 km × 1 km grid over the Greater Athens Area. In their article, a specific PBL was not chosen, but it was confirmed that non-local PBL schemes give the most agreeable solutions when compared with observations.

While different PBL schemes perform well under different circumstances, it was found that local, or TKE closure, schemes performed well during the winter period, and the MYJ scheme (also a local scheme) is preferred for use during spring in the Highveld region. Other studies found similar results pertaining to local schemes. In Southern Italy, it was found that local schemes perform better than non-local schemes when simulating meteorological variables (Tyagi *et al.*, 2018). In addition, Madala *et al.* (2016) concluded that local schemes are more successful in simulating thunderstorm in the West Bengal region of India, as they seem to sustain these pre-storm convective conditions better.

PBLHs were also simulated by the different schemes in the WRF-ARW model, and it was found that their average diurnal variation, daily maximums, and daily minimums agree with results from previous studies. At Irene, June PBLHs at 02 LT were slightly over-estimated by the model, while November PBLHs were under-estimated at the time of both soundings. Gierens *et al.* (2018) conducted a study of PBLH over a two-year period using data from the Welgegund atmospheric measurement station, which is located in the greater Highveld region (approximately 150km from Irene). Results include that lower mean and maximum PBLHs are found in the winter months, where SBL is present from sunset to sunrise and varies below 500m; and where CBL is present from sunrise to sunset and can be as high as 2400m in the winter, and even higher (>3000m) in the summer. Results from this study concur with these findings. International publications exist where PBLHs, simulated by different schemes in the WRF-ARW model, are compared against PBLHs derived from observations. Some report the under-estimation of PBLH in the WRF-ARW model (Banks *et al.,* 2015), while PBLH is overestimated in other regions (Kryza *et al.,* 2015). Considering the fact that observational data lacked temporal resolution, a conclusion regarding the best performing PBL scheme in terms of PBLH simulation could not be made.

6. Conclusion

Four PBL schemes, two local and two non-local, from WRF-ARW model were compared on a 2km x 2km grid over the Highveld region of SA during June and November of 2016. In the research presented, it has been shown that PBL schemes influence meteorological outputs from WRF-ARW model simulations. Since experiment 1 to 4 were all configured in the same way, any variances in meteorological output can be attributed to the PBL and SLSs alone. The WRF-ARW model, with all tested configurations, tended to reproduce temperature, RH, wind speed, and wind direction more accurately during June than during November.

The results in Table 6 indicate that different PBL schemes perform well simulating different variables, especially during June. As an overall recommendation, it is suggested that a local scheme, which uses the TKE method, be used for the Highveld region during winter. During spring, the clearly preferred scheme for the Highveld is the local MYJ scheme.

Table 6. Summary of overall best performing (or preferred) PBL schemes by season and meteorological variable for the Highveld region.

Season	Meteorological variable	Preferred scheme
Winter	Temperature	MYNN/MYJ
	RH	YSU
	Wind speed and direction	MYJ
Spring	Temperature	MYJ
	RH	MYJ (followed by YSU)
	Wind speed and direction	MYJ

The accurate representation of surface meteorological variables are an essential component in successful air quality forecasts. Modelled meteorological, and subsequent air quality simulations, play a very important role in research and air quality related studies in SA. Reports concerning air quality management in pollution priority areas are often based on simulated air quality data. These reports regularly influence high-level decisions, and can have an effect on air quality policies. The results produced by the presented research is expected to contribute to more reliable NWP and air quality simulations in the heavily polluted Highveld region.

Recommendations for further research includes the investigation of PBL performance during other times of the year. Future planned research investigates the effect of different PBL schemes in the simulation of

air quality in the Highveld region, in order to quantify the effects of the different PBL schemes on simulated pollutant concentrations.

7. Acknowledgments

The authors acknowledge The South African Weather Service (SAWS) for the use of their measured meteorological data for all sites for June and November 2016. The WRF-ARW model system software is in the public domain and is freely available at http://www2.mmm.ucar.edu/wrf/users/downloads.html for community use. WRF-ARW model runs were performed on the computer infrastructure Centre for High Performance Computing (CHPC) at the Council for Scientific and Industrial Research (CSIR). This work was supported by SASOL through the Laboratory for Atmospheric Studies (LAS) at the University of Pretoria. We would also like to acknowledge Stephanie Landman from SAWS for helpful discussions.

References

Banks, R., Tiana-Alsina, J., Rocadenbosch, F., Baldasano J., 2015. Performance Evaluation of the Boundary-Layer Height from Lidar and the Weather Research and Forecasting Model at an Urban Coastal Site in the North-East Iberian Peninsula. Boundary-Layer Meteorol. 157(2), 265-292. https://doi.org/10.1007/s10546-015-0056-2.

Banks, R., and Baldasano, J., 2016. Impact of WRF model PBL schemes on air quality simulations over Catalonia, Spain. Sci. Total Environ. 572, 98-113. https://doi.org/10.1016/j.scitotenv.2016.07.167.

Banks, R., Tiana-Alsina, J., Baldasano, J., Rocadenbosch, F., Papayannis, A., Solomos, S., Tzanis, C., 2016. Sensitivity of boundary-layer variables to PBL schemes in the WRF model based on surface meteorological observations, lidar, and radiosondes during the HygrA-CD campaign. Atmos. Res. 176-177, 185-201. https://doi.org/10.1016/j.atmosres.2016.02.024.

Boadh, R., Satyanarayana, A., Rama Krishna, T., Madala, S., 2016. Sensitivity of PBL schemes of the WRF-ARW model in simulating the boundary layer flow parameters for their application to air pollution dispersion modeling over a tropical station. Atmósfera. 29(1), 61-81. https://doi.org/10.20937/ATM.2016.29.01.05.

Borge, R., Alexandrov, V., José del Vas, J., Lumbreras, J., Rodríguez, E., 2008. A comprehensive sensitivity analysis of the WRF model for air quality applications over the Iberian Peninsula. Atmos. Environ. 42(37), 8560-8574. https://doi.org/10.1016/j.atmosenv.2008.08.032.

Brunner, D., Savage, N., Jorba, O., Eder, B., Giordano, L., Badia, A., Balzarini, A., Baró, R., Bianconi, R., Chemel, C., Curci, G., Forkel, R., Jiménez-Guerrero, P., Hirtl, M., Hodzic, A., Honzak, L., Im, U., Knote, C., Makar, P., Manders-Groot, A., van Meijgaard E., Neal, L., Pérez, J., Pirovano, G., San Jose, R., Schröder, W., Sokhi, R., Syrakov, D., Torian, A., Tuccella, P., Werhahn, J., Wolke, R., Yahya, K., Zabkar, R., Zhang, Y., Hogrefe, C., Galmarini, S., 2015. Comparative analysis of meteorological performance of coupled chemistry-

meteorology models in the context of AQMEII phase 2. Atmos. Environ. 115, 470-498. https://doi.org/10.1016/j.atmosenv.2014.12.032.

Cohen, A.E., Cavallo, S.M., Coniglio, M.C., Brooks, H.E., 2015. A Review of Planetary Boundary Layer Parameterization Schemes and Their Sensitivity in Simulating Southeastern U.S. Cold Season Severe Weather Environments. Wea. Forecasting. 30, 591–612. https://doi.org/10.1175/WAF-D-14-00105.1.

Collaud Coen, M., Praz, C., Haefele, A., Ruffieux, D., Kaufmann, P., Calpini, B., 2014. Determination and climatology of the planetary boundary layer height above the Swiss plateau by in situ and remote sensing measurements as well as by the COSMO-2 model. Atmos. Chem. Phys. 14(23), 13205-13221. https://doi.org/10.5194/acp-14-13205-2014.

Colman, B., n.d. "What Is A Good Weather Forecast?" In The Eyes Of A Forecaster. https://sciencepolicy.colorado.edu/socasp/weather1/colman.html (accessed 19 August 2020).

Coniglio, M.C., Correia, J., Marsh, P.T., Kong, F., 2013. Verification of Convection-Allowing WRF Model Forecasts of the Planetary Boundary Layer Using Sounding Observations. Wea. Forecasting. 28, 842–862. https://doi.org/10.1175/WAF-D-12-00103.1.

Crétat, J., Macron, C, Pohl, B, Richard, Y., 2011. Quantifying internal variability in a regional climate model: a case study for Southern Africa. Clim. Dyn. 37, 1335–1356. https://doi.org/10.1007/s00382-011-1021-5.

Crétat, J., Pohl, B., 2012. How Physical Parameterizations Can Modulate Internal Variability in a Regional Climate Model. J. Atmos. Sci. 69, 714–724. https://doi.org/10.1175/JAS-D-11-0109.1.

Crétat, J., Pohl, B., Richard, Y., Drobinski, P., 2012. Uncertainties in simulating regional climate of Southern Africa: sensitivity to physical parameterizations using WRF. Clim. Dyn. 38 (3–4), 613–634. https://doi.org/10.1007/s00382-011-1055-8.

Cuchiara, G.C., Li, X., Carvalho, J., Rappenglück, B., 2014. Intercomparison of planetary boundary layer parameterization and its impacts on surface ozone concentration in the WRF/Chem model for a case study in Houston/Texas. Atmos. Environ. 96, 175–185. https://dx.doi.org/10.1016/j.atmosenv.2014.07.013.

Department of Environmental Affairs (DEA), 2012. Declaration of the Waterberg Priority Area in terms of the National Environmental Management: Air Quality Act No. 39 of 2004. Government Gazette No. 35435. 15 June 2012.

Department of Environmental Affairs and Tourism (DEAT), 2006. Declaration of the Vaal Triangle Air-Shed priority area in terms of section 18 (1) of the National Environmental Management: Air Quality Act (No. 39 of 2004). Government Gazette No. 28732. 21 April 2006.

Department of Environmental Affairs and Tourism (DEAT), 2007. Declaration of the Highveld as a priority area in terms of section 18 (1) of the National Environmental Management: Air Quality Act (No. 39 of 2004). Government Gazette No. 30518. 23 November 2007.

De Lange, A., Garland, R., Dyson, L., 2019. Estimating particulate matter (PM) concentrations from a meteorological index for data-scarce regions: A pilot study. Atmos. Pollut. Res. 10(5), 1553-1564. https://doi.org/10.1016/j.apr.2019.05.004.

Duda, J.D., 2010. A Modelling Study of PBL Heights. https://www.meteor.iastate.edu/~jdduda/portfolio/605_paper.pdf (accessed 14 February 2019).

Dyson, L., van Heerden, J., Sumner, P., 2015. A baseline climatology of sounding-derived parameters associated with heavy rainfall over Gauteng, South Africa. Int. J. Climatol. 35(1), 114-127. https://doi.org/10.1002/joc.3967.

Feig, G., Garland, R., Naidoo, S., Maluleke, A., Van der Merwe, M., 2019. Assessment of changes in concentrations of selected criteria pollutants in the Vaal and Highveld Priority Areas. Clean Air J., 29(2). https://doi.org/10.17159/caj/2019/29/2.7464.

Giannaros, C., Melas, D., Giannaros, T., 2019. On the short-term simulation of heat waves in the Southeast Mediterranean: Sensitivity of the WRF model to various physics schemes. Atmos. Res. 218, 99-116. https://doi.org/10.1016/j.atmosres.2018.11.015.

Gierens, R., Henriksson, S., Josipovic, M., Vakkari, V., van Zyl, P., Beukes, J., Wood, C., O'Connor, E., 2018. Observing continental boundary-layer structure and evolution over the South African savannah using a ceilometer. Theoretical and Applied Climatology, 136(1-2), 333-346, https://doi.org/10.1007/s00704-018-2484-7.

Gilliam, R., Hogrefe, C., Rao, S., 2006. New methods for evaluating meteorological models used in air quality applications. Atmos. Environ. 40(26), 5073-5086. https://doi.org/10.1016/j.atmosenv.2006.01.023.

Govender, K., Sivakumar, V., 2019. A decadal analysis of particulate matter (PM2.5) and surface ozone (O3) over Vaal Priority Area, South Africa. Clean Air J., 29(2). https://doi.org/10.17159/caj/2019/29/2.7578

Gunwani, P., Mohan, M., 2017. Sensitivity of WRF model estimates to various PBL parameterizations in different climatic zones over India. Atmos. Res. 194, 43-65. https://doi.org/10.1016/j.atmosres.2017.04.026.

Hahmann, A., Lennard, C., Badger, J., Vincent, C., Kelly, M., Volker, P., Argent, B., Refslund, J., 2015. Mesoscale modeling for the Wind Atlas of South Africa (WASA) project. DTU Wind Energy E, No. 0050. https://doi.org/10.13140/RG.2.1.3735.6887.

Holzworth, G., 1964. Estimates of Mean Maximum Mixing Depths in the Contiguous United States. Mon. Wea. Rev. 92(5), 235-242.

Hong, S., Lim, J., 2006. The WRF single–moment 6–class microphysics scheme (WSM6). J. Korean Meteorol. Soc. 42, 129–151.

Hong, S., Noh, Y., Dudhia, J., 2006. A New Vertical Diffusion Package with an Explicit Treatment of Entrainment Processes. Mon. Wea. Rev. 134, 2318–2341. https://doi.org/10.1175/MWR3199.1.

Hu, X., Nielsen-Gammon, J.W., Zhang, F., 2010. Evaluation of Three Planetary Boundary Layer Schemes in the WRF Model. J. Appl. Meteorol. Climatol. 49, 1831–1844. https://doi.org/10.1175/2010JAMC2432.1.

Iacono, M.J., Delamere, J.S. Mlawer, E.J., Shephard, M.W., Clough, S.A., Collins, W.D., 2008. Radiative forcing by long–lived greenhouse gases: Calculations with the AER radiative transfer models. J. Geophys. Res. 113, D13103. https://doi.org/10.1029/2008JD009944.

Janjić, Z.I., 1994. The Step-Mountain Eta Coordinate Model: Further Developments of the Convection, Viscous Sublayer, and Turbulence Closure Schemes. Mon. Wea. Rev. 122, 927-945. https://doi.org/10.1175/1520-0493(1994)122<0927:TSMECM>2.0.CO;2.

Jerez, S., López-Romero, J., Turco, M., Lorente-Plazas, R., Gómez-Navarro, J., Jiménez-Guerrero, P., Montávez, J., 2020. On the Spin-Up Period in WRF Simulations Over Europe: Trade-Offs Between Length and Seasonality. J. Adv. Model. 12(4). https://doi.org/10.1029/2019MS001945.

Jin, J., Miller, N.L., Schlegel, N., 2010. Sensitivity Study of Four Land Surface Schemes in the WRF Model. Ad. Meteorol. 2010, Article ID 167436. https://doi.org/10.1155/2010/167436.

Kain, J.S., 2004. The Kain–Fritsch convective parameterization: An update. J. Appl. Meteorol. 43, 170–181. https://doi.org/10.1175/1520-0450(2004)043<0170:TKCPAU>2.0.CO;2.

Kim, Y., Sartelet, K., Raut, J., Chazette, P., 2015. Influence of an urban canopy model and PBL schemes on vertical mixing for air quality modeling over Greater Paris. Atmos. Environ. 107, 289-306. https://doi.org/10.1016/j.atmosenv.2015.02.011.

Korhonen, K., Giannakaki, E., Mielonen, T., Pfüller, A., Laakso, L., Vakkari, V., Baars, H., Engelmann, R., Beukes, J. P., Van Zyl, P. G., Ramandh, A., Ntsangwane, L., Josipovic, M., Tiitta, P., Fourie, G., Ngwana, I., Chiloane, K., Komppula, M., 2014. Atmospheric boundary layer top height in South Africa: measurements with lidar and radiosonde compared to three atmospheric models. Atmos. Chem. Phys. 14, 4263-4278. https://doi.org/10.5194/acp-14-4263-2014.

Kryza, M., Osiadacz, A., Werner, M., Netzel, P., Dore, A., 2015. Comparison of the WRF and Sodar derived planetary boundary layer height. Int. J. Environ. Pollut. 58(1/2), 3.

Kuik, F., Lauer, A., Beukes, J.P., Van Zyl, P.G., Josipovic, M., Vakkari, V., Laaks, L., Feig, G.T., 2015. The anthropogenic contribution to atmospheric black carbon concentrations in southern Africa: a WRF-Chem modelling study. Atmos. Chem. Phys. 15, 8809-8830. https://doi.org/10.5194/acp-15-8809-2015.

Liu, S., Liang, X., 2010. Observed Diurnal Cycle Climatology of Planetary Boundary Layer Height. J. Clim. 23(21), 5790-5809. https://doi.org/10.1175/2010JCLI3552.1.

López-Bravo, C., Caetano, E., Magaña, V., 2018. Forecasting Summertime Surface Temperature and Precipitation in the Mexico City Metropolitan Area: Sensitivity of the WRF Model to Land Cover Changes. Front. Earth Sci. Volume 6, Article 6. https://doi.org/10.3389/feart.2018.00006.

Madala, S., Satyanarayana, A., Srinivas, C., Tyagi, B., 2016. Performance evaluation of PBL schemes of ARW model in simulating thermo-dynamical structure of pre-monsoon convective episodes over Kharagpur using STORM data sets. Pure Appl. Geophys. 173(5), 1803-1827. https://doi.org/10.1007/s00024-015-1210-y.

Nakanishi, M., Niino, H., 2006. An Improved Mellor–Yamada Level-3 Model: Its Numerical Stability and Application to a Regional Prediction of Advection Fog. Boundary-Layer Meteorol. 119, 397. https://doi.org/10.1007/s10546-005-9030-8.

Ngailo, T.J., Shaban, N., Reuder, J., Mesquita, M.D.S., Rutalebwa, E., Mugume, I., Sangalungembe, C., 2018. Assessing Weather Research and Forecasting (WRF) Model Parameterization Schemes Skill to Simulate Extreme Rainfall Events over Dar es Salaam on 21 December 2011. J. Geosci. Environ. Prot. 6, 36-54. https://doi.org/10.4236/gep.2018.61003.

Pérez, C., Jiménez, P., Jorba, O., Sicard, M., Baldasano, J.M., 2006. Influence of the PBL scheme on high-resolution photochemical simulations in an urban coastal area over the western Mediterranean. Atmos. Environ. 40(27), 5274–5297. https://doi.org/10.1016/j.atmosenv.2006.04.039.

Pleim, J.E., 2007. A Combined Local and Nonlocal Closure Model for the Atmospheric Boundary Layer. Part I: Model Description and Testing. J. Appl. Meteorol. Clim. 46, 1383–1395. https://doi.org/10.1175/JAM2539.1.

Pohl, B., Rouault, M., Roy, S.S., 2014. Simulation of the annual and diurnal cycles of rainfall over South Africa by a regional climate model. Clim. Dyn. 43(7–8), 2207–2226. https://doi.org/10.1007/s00382-013-2046-8.

Politi, N., Nastos, P.T., Sfetsos, A., Vlachogiannis, D., Dalezios, N.R., 2018. Evaluation of the AWR-WRF model configuration at high resolution over the domain of Greece. Atmos. Res. 208, 229-245. https://doi.org/10.1016/j.atmosres.2017.10.019.

Ratna, S.B., Ratnam, J.V., Behera, S.K., Rautenbach, C.J., Ndarana, T., Takashi, K., Yamagata, T., 2014. Performance assessment of three convective parameterization schemes in WRF for downscaling summer rainfall over South Africa. Clim. Dyn. 42(11–12), 2931–2953. https://doi.org/10.1007/s00382-013-1918-2.

Ratnam, J.V., Behera, S.K., Ratna, S.B., Rautenbach, C.J., Lennard, C., Luo, J., Masumoto, Y., Takahashi, K., Yamagata T., 2013. Dynamical Downscaling of Austral Summer Climate Forecasts over Southern Africa Using a Regional Coupled Model. J. Climate. 26, 6015–6032. http://doi.org/10.1175/JCLI-D-12-00645.1.

Ratnam, J.V., Behera, S.K., Doi, T., Ratna, S.B., Landman, W.A., 2016. Improvements to the WRF Seasonal Hindcasts over South Africa by Bias Correcting the Driving SINTEX-F2v CGCM Fields. J. Clim. 29(8), 2815–2829. https://doi.org/10.1175/JCLI-D-15-0435.1.

Ritter, M., Müller, M.D., Jorba, O., 2013. Impact of chemical and meteorological boundary and initial conditions on air quality modeling: WRF-Chem sensitivity evaluation for a European domain. Meteorol. Atmos. Phys. 119, 59-70. https://doi.org/10.1007/s00703-012-0222-8.

Skamarock, W. C., Klemp, J.B., Dudhia, J.D., Gill, O., Barker, D.M., Duda, M.G., Huang, X.Y., Wang, W., Powers, J.G., 2008. A Description of the Advanced Research WRF Version 3. NCAR Tech. Note NCAR/TN-475+STR, https://doi.org/10.5065/D68S4MVH.

[dataset] Saha, S., Moorthi, S., Wu, X., Wang, J., Nadiga, S., Tripp, P., Behringer, D., Hou, Y., Chuang, H., Iredell, M., Ek, M., Meng, J., Yang, R., Mendez, M. P., van den Dool, H., Zhang, Q., Wang, W., Chen, M., Becker, E., 2011. NCEP Climate Forecast System Version 2 (CFSv2) 6-hourly Products. Research Data Archive at the National Center for Atmospheric Research, Computational and Information Systems Laboratory. https://doi.org/10.5065/D61C1TXF.

Seibert, P., Beyrich, F., Gryning, S., Joffre, S., Rasmussen, A., Tercier, P., 2000. Review and intercomparison of operational methods for the determination of the mixing height. Atmos. Environ. 34, 1001-1027. https://doi.org/10.1016/S1352-2310(99)00349-0.

Tewari, M., Chen, F., Wang, W., Dudhia, J., LeMone, M. A., Mitchell, K., Ek, M., Gayno, G., Wegiel, J., Cuenca, R.H., 2004. Implementation and verification of the unified NOAH land surface model in the WRF model. 20th conference on weather analysis and forecasting/16th conference on numerical weather prediction.

Tyagi, B., Magliulo, V., Finardi, S., Gasbarra, D., Carlucci, P., Toscano, P., Zaldei, A., Riccio, A., Calori, G., D'Allura, A., Gioli, B., 2018. Performance analysis of planetary boundary layer parameterization schemes in WRF modeling set up over southern Italy. Atmosphere. 9(7), 272. https://doi.org/10.3390/atmos9070272.

Tyson, P.D., Kruger, F.J. and Louw, C.W. (eds)., 1988. Atmospheric Pollution and its Implications in the Eastern Transvaal Highveld, South African National Scientific Programmes Report No. 150, Council for Scientific and Industrial Research, Pretoria

Tyson, P.D., Preston-Whyte, R.A., 2000. The weather and climate of Southern Africa. Oxford University Press Southern Africa, Cape Town, South Africa. ISBN: 978-0-195-71806-5.

Venter, A., Vakkar, V., Beukes, J., Van Zyl, P., Laakso, H., Mabaso, D., Tiitta, P., Josipovic, M., Kulmala, M., Pienaar, J., Laakso, L., 2012. An air quality assessment in the industrialised western Bushveld Igneous Complex, South Africa. S. Afr. j. sci., 108(9/10). http://dx.doi.org/10.4102/sajs.v108i9/10.1059.

Wallace, J., Hobbs, P., 2006. Atmospheric Science. Amsterdam: Amsterdam.

Xie, B., Fung, J.C.H., Chan, A., Lau, A., 2012. Evaluation of nonlocal and local planetary boundary layer schemes in the WRF model. J. Geophys. Res. 117, D12103. https://doi.org/10.1029/2011JD017080.

Zeyaeyan, S., Fattahi, E., Ranjbar, A., Azadi, M., Vazifedoust, M., 2017. Evaluating the Effect of Physics Schemes in WRF Simulations of Summer Rainfall in North West Iran. J. Clim. 5(3), 48. https://doi.org/10.3390/cli5030048.

Appendix A: Day-to-day variability in WRF-ARW simulations

This appendix serves as verification that the setup of the long-term WRF-ARW simulation reflects the day-to-day variations of meteorological conditions. Synoptic charts issued by the South African Weather Service (SAWS) (Available from https://www.weathersa.co.za/home/historicalsynoptic) are used together with hourly time series plots of temperature, relative humidity, wind speed, and wind direction for June 2016 at Ermelo. Synoptic circulations, and accompanying data, are discussed in short. While the data in this appendix only considers one site (Ermelo), the above-mentioned meteorological characteristics were present to differing degrees at all sites, during June 2016. June 2016 was chosen as the period of interest for the purpose of this Appendix because there were significant synoptic scale weather systems that moved over the study region during this period. This allowed for the investigation of the daily variation of the meteorological parameters.

Day-to-day variations are shown by considering a few synoptic scale systems which occurred during the time of simulation. The systems considered include a ridging high-pressure system from west to east of South Africa from 3 to 4 June 2016 (Fig. A.1; Period A), a cold front followed by a ridging high from 10 to 13 June 2016 (Fig A.3; Period B), and a ridge over the eastern parts of the country from 15 to 16 June 2016 (Fig A.4; Period C).

The three weather systems show that synoptic systems which influence the study region, are simulated by the model, even though their impact is not always reproduced perfectly. What is important to note, is that although simulations sometimes (as in Period C), deviate from the observed weather patterns, the simulations quickly recover, and perform well in the periods thereafter. This is a clear indication that daily variation in meteorological conditions are adequately captured by the model setup and simulations. The daily variation in meteorological variables are also clearly visible in the time series plots (Fig. A.2).

a. Ridging high-pressure system from west to east of the country from 3 to 4 June 2016 (Period A)

A high-pressure system west of the country on 3 June 2016, ridged eastwards on 4 June 2016 (Fig. A.1). Westerly winds (between 225 and 315°) are prevalent in the observational, as well as the simulated wind direction data, from 3 to 4 June 2016 (Fig. A.2). This dry westerly wind caused maximum humidity on 3 June to be only about 60% (seen in observed and simulated data). The observations and simulation show

that the daily humidity is much higher on the 2nd and 4th of June 2016. On the 4th of June, the observed wind directions change to be predominantly between 50°and 150° (north-easterly to south-easterly) and this same change is captured by the simulation. The change in wind direction is consistent with the wind directions expected over the interior with a high ridging over the eastern parts of the country.

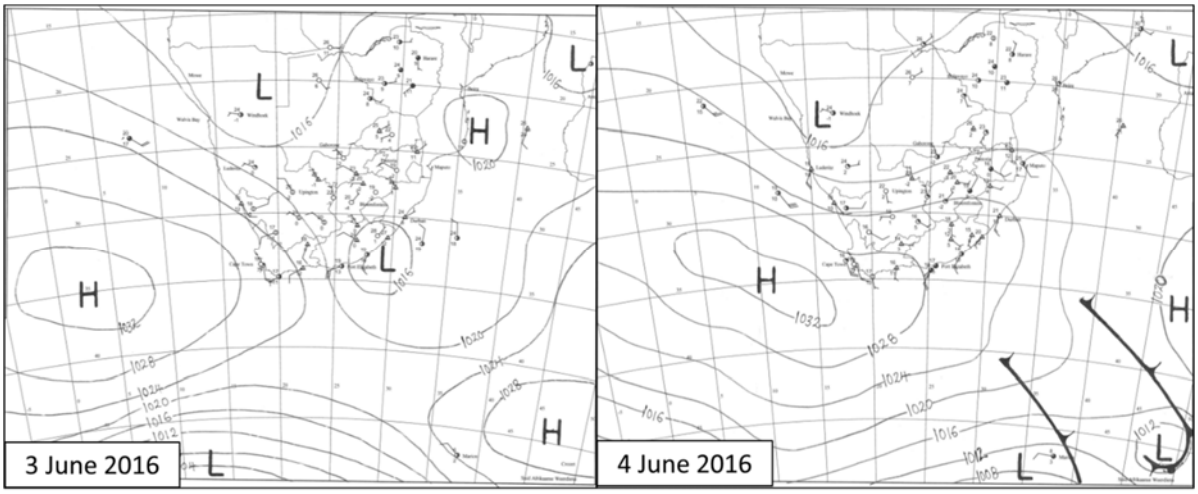

Figure A.1. Surface synoptic charts for 3 and 4 June 2016 (Period A).

b. Cold front followed by a ridging high from 10 to 13 June 2016 (Period B)

Between 10 June and 11 June 2016, a front is situated over the southern parts of the country, approching the Highveld. Wind direction shifts from south-westerly to easterly, and wind speeds are also stronger than usual, as the front moves through. The cold front is followed by a ridging high, which established itself east of the country on the 13th of June (Fig. A.3).

Figure A.2 shows a time series of observed and simulated termperature data. From the 12th to 13th of June, temperatures drop significantly as cloudy conditions, associated with ridging high, dominates. During this period, relative humidity starts increasing as the high ridges east of the country. Daily maximum and minimum humidities much higher than the rest of the month during this period and is caused by the onshore (north-easterly) flow of moist air (Fig. A.2).

While temperature, relative humidity and wind directions are well-simulated during period B, wind speeds are under-estimated during this period, especially on the 12th of June.

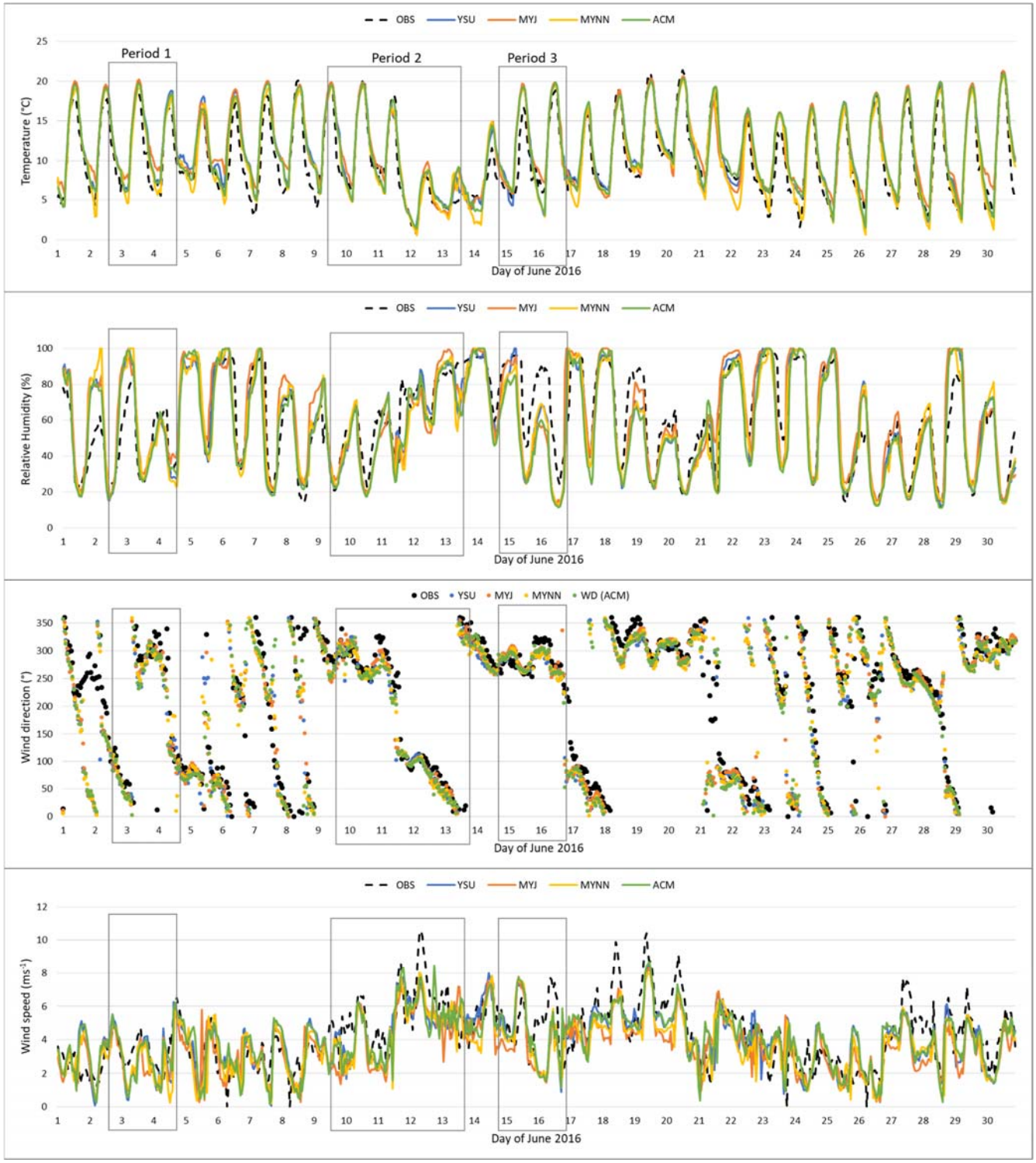

Figure A.2. Time-series plots of hourly observed (OBS) and simulated (YSU, MYJ, MYNN and ACM) temperature, relative humidity, wind direction,and wind speed for Ermelo during June 2016. Rectangles on the plots indicate period A, B and C, respectively.

c. Ridge over the eastern parts of the country from 15 to 16 June 2016 (Period C)

The final system considered is the ridge over the eastern parts of the country on 15 June (Fig. A.4). Circulation around this small ridge (indicated on Fig. A.4) caused north-westerly/westerly winds over the Highveld of the country, as well as an increase in relative humidity.

WRF-ARW did not simulated the impact of the ridge over the Highveld adequately; therefore, relative humidity was under-estimated at Ermelo on 15 June 2016 (Fig. A.2). During the day of the 16th, simulated relative humidity patterns recover. This supports the statement that the model simulation captures daily variability in meteorology.

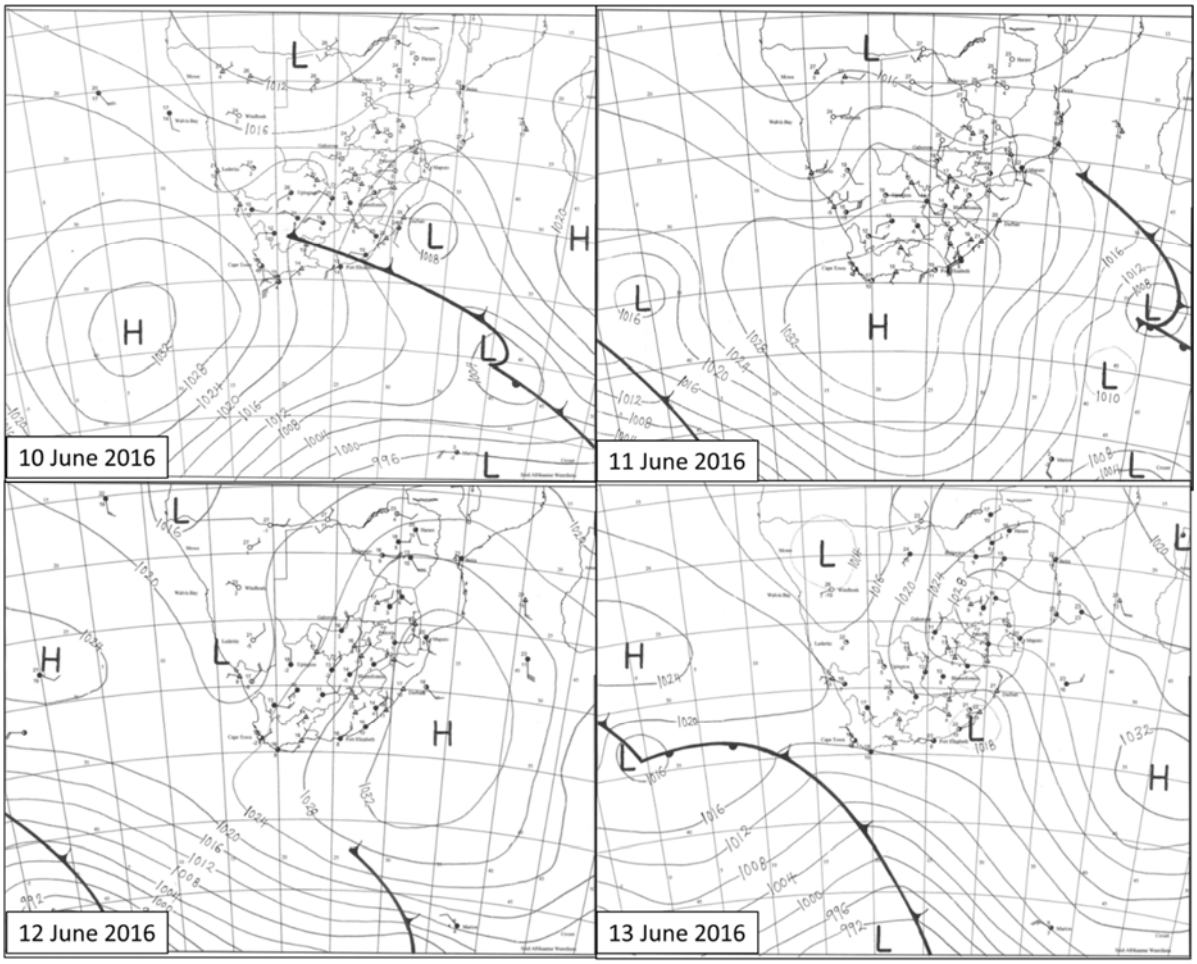

Figure A.3. Surface synoptic charts for 10 June to 13 June 2016 (Period B).

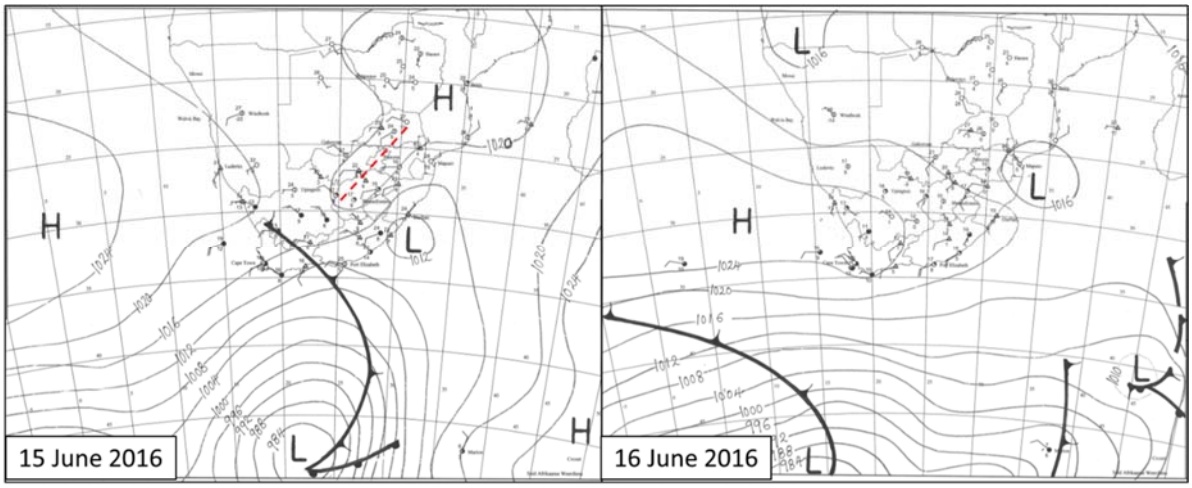

Figure A.4. Surface synoptic charts for 15 and 16 June 2016 (Period C).

Appendix B: Vertical potential temperature profiles

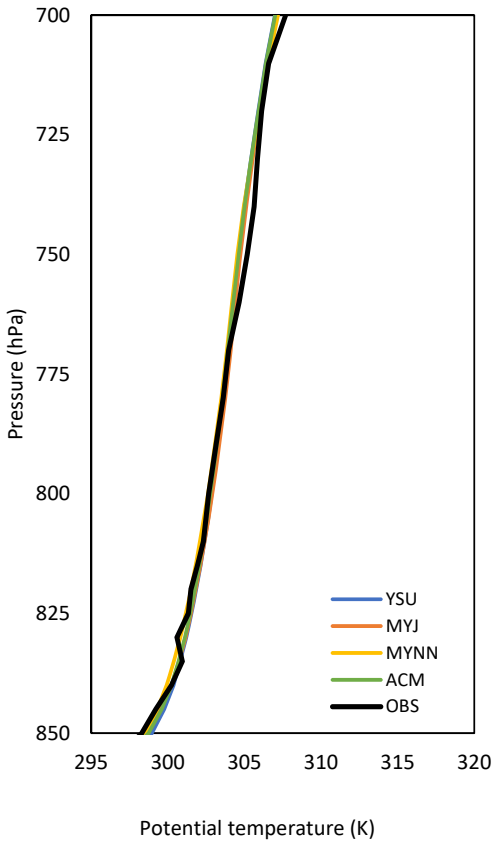

Figure B.1. Average observed (OBS) and simulated (YSU, MYJ, MYNN, ACM) vertical profiles of calculated potential temperature during June at 02 LT.

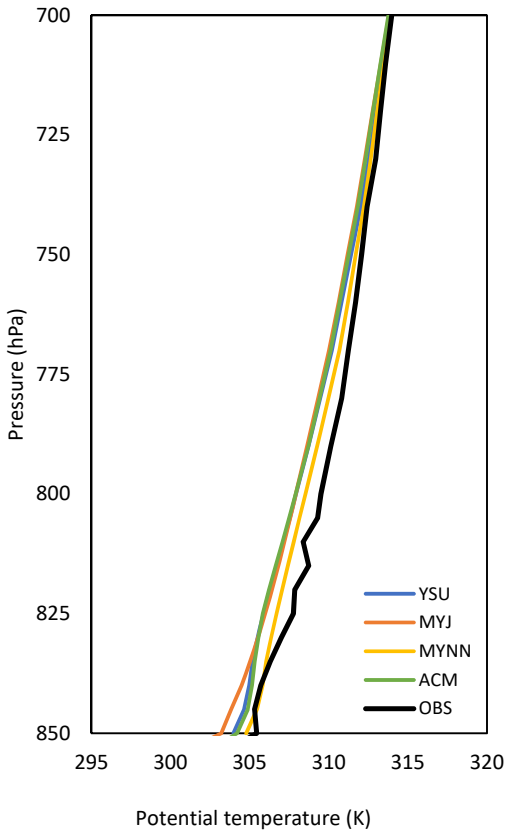

Figure B.2. Average observed (OBS) and simulated (YSU, MYJ, MYNN, ACM) vertical profiles of calculated potential temperature during November at 02 LT.

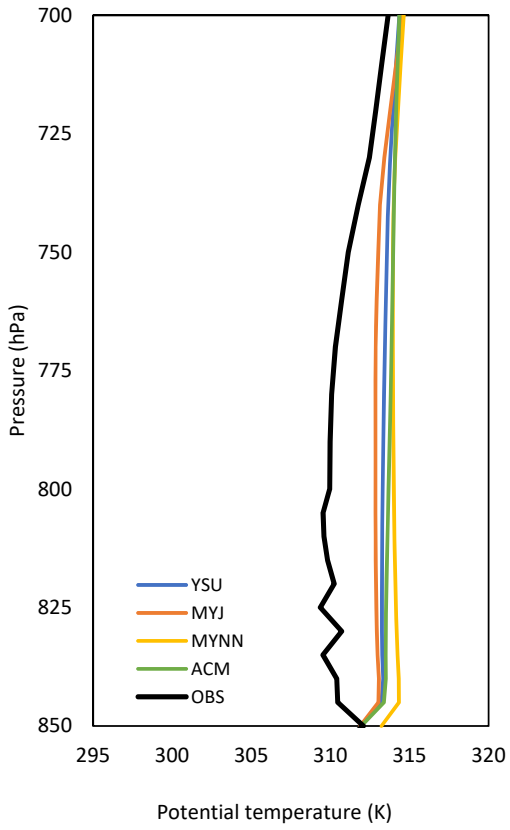

Figure B.3. Average observed (OBS) and simulated (YSU, MYJ, MYNN, ACM) vertical profiles of calculated potential temperature during November at 14 LT.